JGR Oceans

RESEARCH ARTICLE
10.1029/2022JC018999

Seasonal Dynamics of Dissolved Iron on the Antarctic Continental Shelf: Late-Fall Observations From the Terra Nova Bay and Ross Ice Shelf Polynyas

P. N. Sedwick[1], B. M. Sohst[1], C. O'Hara[1], S. E. Stammerjohn[2], B. Loose[3], M. S. Dinniman[4], N. J. Buck[5,6], J. A. Resing[5,6], and S. F. Ackley[7]

[1]Department of Ocean and Earth Sciences, Old Dominion University, Norfolk, VA, USA, [2]Institute of Arctic and Alpine Research, University of Colorado, Boulder, CO, USA, [3]Graduate School of Oceanography, University of Rhode Island, Narragansett, RI, USA, [4]Center for Coastal Physical Oceanography, Old Dominion University, Norfolk, VA, USA, [5]Cooperative Institute for Climate, Oceans, and Ecosystem Studies, University of Washington, Seattle, WA, USA, [6]NOAA Pacific Marine Environmental Laboratory, Seattle, WA, USA, [7]Center for Advanced Measurements in Extreme Environments, University of Texas at San Antonio, San Antonio, TX, USA

Key Points:

- Late-fall observations from two Ross Sea polynyas reveal variability in the extent of vertical mixing and distributions of dissolved iron
- In Terra Nova Bay, katabatic winds and sea ice formation drove deep convective mixing that had extended into dense, iron-rich Shelf Waters
- Vertical mixing was less advanced in the Ross Ice Shelf polynya, suggesting that vertical resupply of iron mainly occurs later in winter

Correspondence to:
P. N. Sedwick,
psedwick@odu.edu

Citation:
Sedwick, P. N., Sohst, B. M., O'Hara, C., Stammerjohn, S. E., Loose, B., Dinniman, M. S., et al. (2022). Seasonal dynamics of dissolved iron on the Antarctic continental shelf: Late-fall observations from the Terra Nova Bay and Ross Ice Shelf polynyas. *Journal of Geophysical Research: Oceans*, *127*, e2022JC018999. https://doi.org/10.1029/2022JC018999

Received 21 JUN 2022
Accepted 23 SEP 2022

Abstract Over the Ross Sea shelf, annual primary production is limited by dissolved iron (DFe) supply. Here, a major source of DFe to surface waters is thought to be vertical resupply from the benthos, which is assumed most prevalent during winter months when katabatic winds drive sea ice formation and convective overturn in coastal polynyas, although the impact of these processes on water-column DFe distributions has not been previously documented. We collected hydrographic data and water-column samples for trace metals analysis in the Terra Nova Bay and Ross Ice Shelf polynyas during April–May 2017 (late austral fall). In the Terra Nova Bay polynya, we observed intense katabatic wind events, and surface mixed layer depths varied from ~250 to ~600 m over lateral distances <10 km; there vertical mixing was just starting to excavate the dense, iron-rich Shelf Waters, and there was also evidence of DFe inputs at shallower depths in the water column. In the Ross Ice Shelf polynya, wind speeds were lower, mixed layers were <300 m deep, and DFe distributions were similar to previous, late-summer observations, with concentrations elevated near the seafloor. Corresponding measurements of dissolved manganese and zinc, and particulate iron, manganese, and aluminum, suggest that deep DFe maxima and some mid-depth DFe maxima primarily reflect sedimentary inputs, rather than remineralization. Our data and model simulations imply that vertical resupply of DFe in the Ross Sea occurs mainly during mid-late winter, and may be particularly sensitive to changes in the timing and extent of sea ice production.

Plain Language Summary The Ross Sea is among the most productive areas on the Antarctic continental shelf. Here, primary production during the austral summer season is limited by the availability of dissolved iron (DFe), an essential micronutrient. A major source of DFe to Ross Sea surface waters is thought to be deep convective mixing, driven by strong, cold katabatic (offshore) winds and associated sea ice formation during austral winter (~May–September). This mixing is assumed to deliver DFe-rich bottom waters to the surface, particularly in coastal polynyas, where sea ice is formed and exported northwards. However, the impact of winter mixing on the distribution of DFe has not been previously documented in the Ross Sea. We report such observations from the Terra Nova Bay polynya (TNBP) and Ross Ice Shelf polynya (RISP) at the onset of winter (late April to late May) 2017. In the TNBP, intense katabatic winds and vigorous sea ice formation drove convective mixing that was penetrating into dense, DFe-rich bottom waters. In the RISP, with milder local winds and less sea ice formation, vertical mixing had not reached DFe-rich deep waters. Our results indicate that deep mixing does indeed supply substantial DFe to Ross Sea surface waters, although primarily in mid-late winter (~June–September).

1. Introduction

The biological consumption of nutrients from waters of the "lower cell" of the meridional overturning circulation that upwell south of the Antarctic Polar Front exerts an important control on the ocean-atmosphere balance of carbon dioxide (Kwon et al., 2009; Marinov et al., 2006). A significant proportion of this primary production occurs in polynyas over the Antarctic continental shelves (Arrigo, vanDijken, & Bushinsky, 2008; Arrigo et al., 2015; Laufkoetter et al., 2018). The Ross Sea continental shelf is among the most productive of these

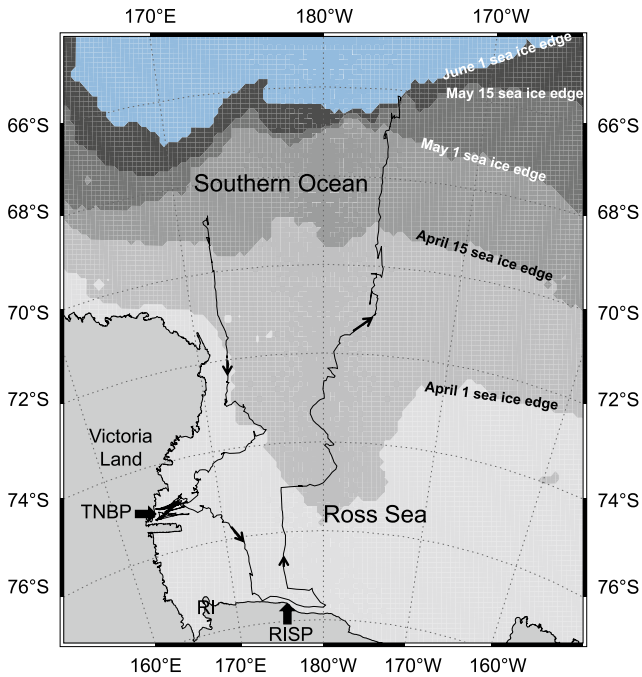

Figure 1. Within-ice cruise track of the PIPERS expedition aboard RVIB *Nathaniel B. Palmer*. Background gray shading corresponds to Advanced Microwave Scanning Radiometer 2 sea-ice extent for April 1, April 15, May 1, May 15, and June 1, 2017 (defined with a 15% concentration cutoff). Shown are locations of Terra Nova Bay polynya (TNBP), Ross Island (RI), and Ross Ice Shelf polynya (RISP). Base figure provided courtesy of Ted Maksym.

shelf regions, accounting for a net primary production (NPP) of around ~20 Tg C y^{-1}, compared with an estimated total NPP of ~1,950 Tg C y^{-1} for the Southern Ocean south of 50°S; as such, the Ross Sea shelf supports ~1% of Southern Ocean NPP, although it accounts for only ~0.2% of the open-water area of the Southern Ocean (Arrigo, vanDijken, & Bushinsky, 2008; Arrigo, van Dijken, & Long, 2008). In contrast to much of the open Southern Ocean, where chronic iron deficiency limits primary production (Boyd et al., 2010; Coale et al., 2004), the Ross Sea shelf appears subject to seasonal iron limitation, as a result of phytoplankton consuming dissolved iron (DFe) from surface waters during the austral summer growing season (Arrigo et al., 2003; Coale et al., 2003; Fitzwater et al., 2000; Sedwick et al., 2000, 2011). Under this scenario, the DFe that sets the magnitude of annual primary production is supplied from the melting of sea ice and glacial ice, the intrusion and upwelling of Circumpolar Deep Water, and the vertical resupply of iron-rich bottom waters (Gerringa et al., 2015; Hatta et al., 2017; Marsay et al., 2014, 2017; McGillicuddy et al., 2015; Sedwick et al., 2011).

It has been assumed that this vertical resupply of DFe occurs primarily during the winter months, when katabatic winds drive sea ice formation and deep convective overturn in the coastal polynyas of the southwestern Ross Sea (Boyd, 2002; McGillicuddy et al., 2015; Sedwick et al., 2011). However, the timing and impact of these processes on the water-column distribution of DFe have not been previously documented, and such information is required for a full understanding of the seasonal dynamics of iron and its impact on biological production on the Ross Sea continental shelf. To this end, we collected hydrographic observations and water-column samples for trace element analysis from the Terra Nova Bay polynya and Ross Ice Shelf polynya during the late fall, as part of the *Polynyas and Ice Production Evolution in the Ross Sea* (PIPERS) expedition in April–June 2017 (Ackley et al., 2020). Here, we present our results for DFe in the water column, as well as complementary data for dissolved manganese and zinc, and particulate iron, manganese, and aluminum, and discuss the implications of these data for the seasonal dynamics of iron over the Ross Sea continental shelf.

2. Materials and Methods

2.1. Sample Collection

Seawater samples and associated field observations were collected over the Ross Sea continental shelf between April 23 and May 28, 2017, during the PIPERS field program on cruise NBP17-04 of the RVIB *Nathaniel B. Palmer*. This 62-day expedition examined a broad range of questions concerning interactions between ocean, sea ice, and atmosphere in the Ross Sea during the autumn-winter period, with a particular focus on the Terra Nova Bay polynya and Ross Ice Shelf polynya (Ackley et al., 2020; Figure 1). Water-column samples for analysis of dissolved and particulate trace elements, and continuous profiles of temperature and salinity were collected using a trace-metal clean conductivity-temperature-depth (CTD) sensor (SBE 19 plus, SeaBird Electronics) mounted on a custom-built trace-metal clean rosette (SeaBird Electronics) fitted with custom-modified 5-L Teflon-lined external-closure Niskin-X samplers (General Oceanics), deployed using a non-metallic line with a polymer jacket (Marsay et al., 2014). Our collection and processing of samples for analysis of trace metals largely followed protocols recommended by the GEOTRACES program (Cutter et al., 2017).

Upon recovery, the Niskin-X water samplers were transferred into a shipboard clean-air container laboratory, where seawater samples were filtered through pre-cleaned 0.2 µm pore AcroPak Supor filter capsules (Pall) using filtered nitrogen gas. Filtrate was collected in acid-cleaned 125 ml low-density polyethylene bottles (Nalgene) and acidified to pH 1.8 by the addition of ultrapure hydrochloric acid (Fisher Optima) for shore-based determinations of dissolved iron (DFe), manganese (DMn), and zinc (DZn). In addition, from selected Niskin-X samples, a pre-cleaned perfluoroalkoxy alkane (PFA) cylindrical reservoir (Savillex) was filled with approximately 1.8 L of unfiltered seawater, which was passed through sequential 2 µm-pore and 0.2 µm-pore acid-cleaned 47-mm

diameter polycarbonate membrane filters (Poretics) mounted in an in-line PFA filter holder (Savillex) using filtered compressed air. The membrane filters were then rinsed with 200 ml of ultrapure deionized water (Barnstead Nanopure) that had been adjusted to pH 8 with ultrapure ammonium hydroxide solution (Fisher Optima grade), to remove sea salt that may interfere with the X-ray fluorescence analysis. We note that this rinse volume is greater than that typically used (if at all) for particles filtered for analysis by other methods such as ICP-MS (e.g., see Cutter et al., 2017), and may therefore result in the loss of some portion of the most labile fraction of particulate trace elements on the filters. The rinsed filters were then placed in pre-cleaned polystyrene petri dishes (Fisher) and air-dried under a Class-100 clean-air bench. Dried filters were stored in the sealed petri dishes inside a desiccator at room temperature for shore-based analysis of particulate iron (PFe), manganese (PMn), and aluminum (PAl), as described in Section 2.2.

In addition to the trace-metal CTD-rosette sampling, hydrographic data and water-column samples for analysis of other species (e.g., oxygen and noble gases; see Ackley et al., 2020; Loose et al., 2022) were collected using the ship's conventional CTD-rosette which was fitted with 12-L Ocean Test Equipment samplers. However, the conventional CTD-rosette sampling stations were not always located adjacent to the trace-metal CTD-rosette stations, which limits our ability to directly compare data sets from the different sampling systems.

2.2. Sample Analysis

Concentrations of DFe, DMn, and DZn were measured using a sector-field inductively coupled plasma mass spectrometer (Thermo Fisher Scientific ElementXR) with an in-line separation-preconcentration system (Elemental Scientific SeaFAST SP3), following a modification of the method of Lagerström et al. (2013). Calibration standards were prepared in low-analyte concentration seawater, for which initial concentrations were determined using the method of standard additions, with scandium used as an internal standard. Analytical blank concentrations were assessed by applying the in-line separation-preconcentration procedure including all reagents and loading air in place of the seawater sample (air blank), with the following mean blank concentrations: 0.002 nM DFe, <0.001 nM DMn, and 0.001 nM DZn. Limits of detection, defined as the concentration equivalent to three times the standard deviation on the mean blank (n = 12), were 0.042 nM DFe, 0.003 nM DMn, and 0.018 nM DZn. Estimated analytical precision is expressed as the average of the relative standard deviations obtained for replicate (separate-day) analyses of 58 different samples, as follows: 8.0% for DFe, 1.8% for DMn, and 5.8% for DZn. In terms of external consistency, we obtained the following mean concentrations for the GEOTRACES GSP seawater consensus material: 0.187 ± 0.037 nM DFe (n = 17; consensus value 0.155 ± 0.045 nM), 0.789 ± 0.016 nM DMn (n = 19; consensus value 0.778 ± 0.034 nM), and 0.015 ± 0.003 nM DZn (n = 3; consensus value 0.030 ± 0.052 nM).

Concentrations of PFe, PMn, and PAl in particles collected on 2 μm-pore and 0.2 μm-pore membrane filters were determined using energy dispersive X-ray fluorescence using a Thermo Fisher Scientific Quant'X equipped with a rhodium target X-ray tube and lithium-drifted solid-state detector, following the method of Buck et al. (2021). Calibrations were performed using commercially available thin-film standards (MicroMatter Inc.), as well as low-concentration standards for PFe and PMn (<1,000 ng cm^{-2}) that were prepared as described by Buck et al. (2021). Field blanks, for which acid-cleaned 0.2 μm-pore and 2 μm-pore polycarbonate membranes were mounted in the filtration assembly, rinsed with 200 ml of pH 8 ammonium hydroxide solution, then air dried and stored as for the samples, yielded the following measured blank concentrations that were subtracted from corresponding sample concentrations: 4.5/5.1 ng cm^{-2} Fe (0.2 μm/2 μm), below detection limit for Mn (0.2 μm/2 μm), and 11.78/11.77 ng cm^{-2} Al (0.2 μm/2 μm). Detection limits were defined as three times the square root of the background intensity measured for a standard of known concentration (Buck et al., 2021), which yields 0.95 ng cm^{-2} Fe (equivalent to ∼0.13 nM PFe), 1.27 ng cm^{-2} Mn (equivalent to ∼0.18 nM PMn), and 9.4 ng cm^{-2} Al (equivalent to ∼2.8 nM PAl). Precision and accuracy of the method were assessed from multiple analyses of a sample of the NIST-2783 standard reference material (air particulate on filter media), with mean recoveries of 108 ± 2.6% for Fe, 104 ± 2.5% for Mn, and 92 ± 3.5% for Al (n = 320 analyses). The data presented here for PFe, PMn, and PAl represent the sum of the concentrations of the particles separated on 2 μm-pore and 0.2 μm-pore filters; that is, they represent the concentrations of particles in the >0.2 μm size range.

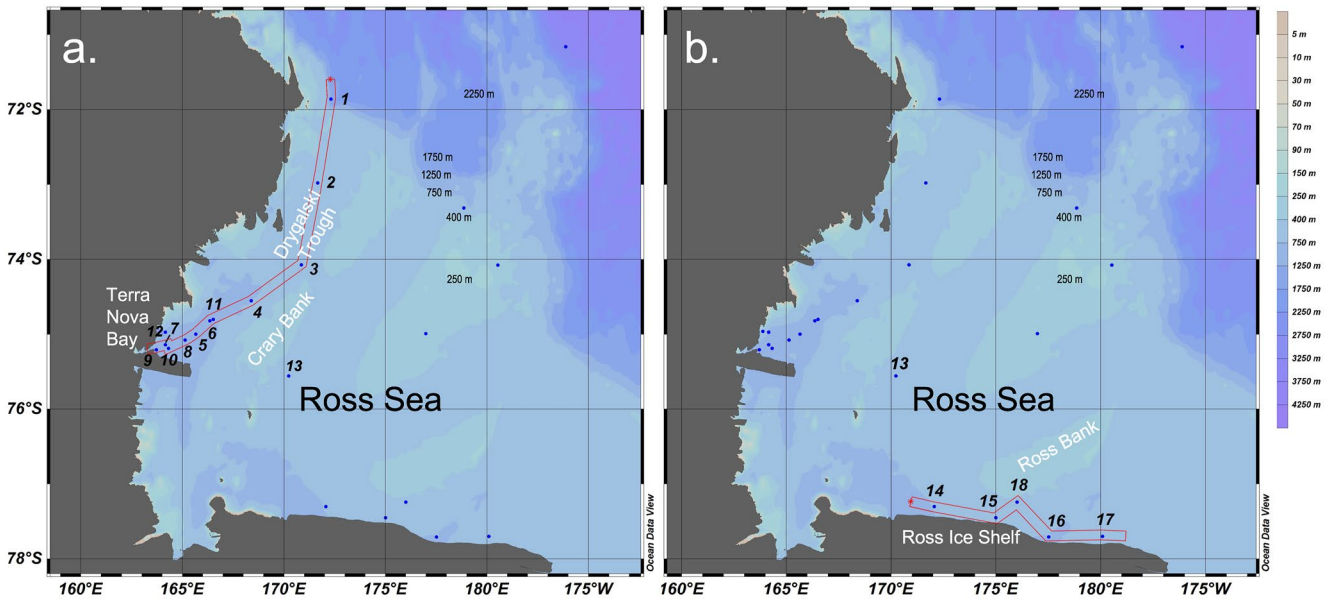

Figure 2. Map showing locations of PIPERS trace-metal CTD sampling stations along (a) Drygalski Trough-Terra Nova Bay transect (stations 1–11) and (b) Ross Ice Shelf transect (stations 14–17). Also shown is location of station 13, southeast of Crary Bank.

3. Results and Discussion

3.1. Physical Context of the Study

During the austral summer, much of the Ross Sea continental shelf is typically free of sea ice (Comiso et al., 2011; Parkinson, 2019), and primary production rates are widely limited by low concentrations of DFe (<0.2 nM) in the euphotic zone (Coale et al., 2003; Fitzwater et al., 2000; Sedwick et al., 2000, 2011). Convective overturn is presumed to replenish the upper water column with benthic iron in the late autumn and winter months (Boyd, 2002; McGillicuddy et al., 2015; Sedwick et al., 2000), particularly within the coastal polynyas of Terra Nova Bay and adjacent to the Ross Ice Shelf, where katabatic winds drive intense sea-ice production and associated brine rejection that results in vertical mixing (Fusco et al., 2009; Kwok, 2005; Rack et al., 2021; Thompson et al., 2020). Consequently, our efforts to document the seasonal vertical resupply of DFe on the Ross Sea shelf focused on two portions of the PIPERS cruise track: (a) a quasi-meridional transect that followed the Drygalski Trough from the shelf break into Terra Nova Bay (Figure 2a), and (b) a quasi-zonal transect that was completed immediately to the north of the Ross Ice Shelf (Figure 2b).

The PIPERS field program allowed for the first shipboard observations from the Ross Sea continental shelf during the sea-ice growth season since 1998. In contrast to the consistent positive trend in sea ice cover observed from 1979 through 2015, the PIPERS cruise period was anomalous in that the Ross Sea experienced record lows in sea ice area in spring 2016 and fall 2017 (and also in successive years), which is thought to reflect a combination of poleward heat advection, surface warming, and weakened ocean stratification that have been linked to modes of atmospheric variability (Meehl et al., 2019; Parkinson, 2019; Schlosser et al., 2018; Turner et al., 2017). This situation contributed to increased production and export of sea ice in coastal polynyas during the cruise period, whereas airborne observations from austral spring 2017 suggest that the winter sea ice production over the Ross Sea shelf was not anomalous (Ackley et al., 2020). We are not able to rigorously assess the representativeness of the fall 2017 season in terms of convective vertical mixing within the Ross Sea coastal polynyas, although the relatively late advance of sea ice during fall 2017 implies that convective overturn may have been substantially delayed or retarded, relative to preceding years.

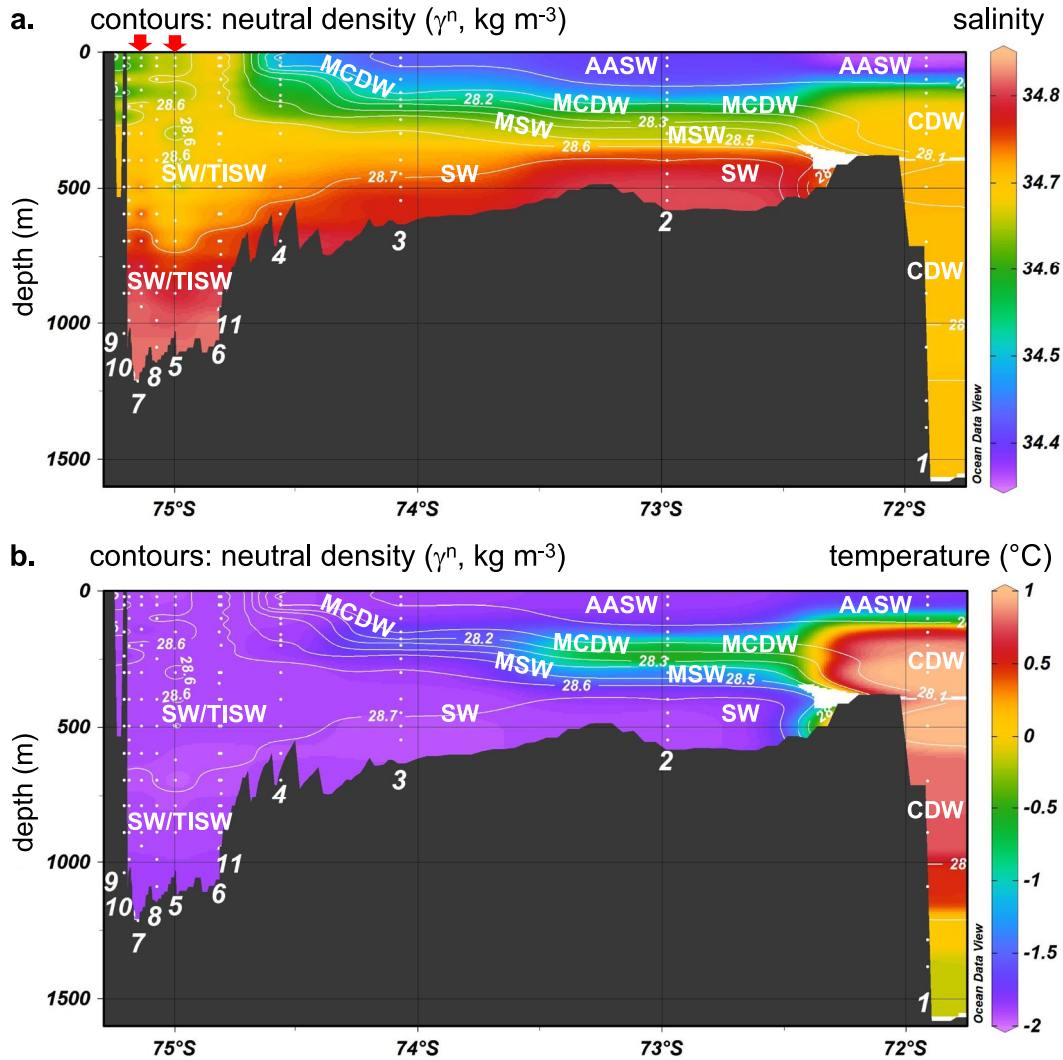

Figure 3. Interpolated sections of (a) salinity and (b) temperature along the Drygalski Trough-Terra Nova Bay transect (stations 1–11), showing Antarctic Surface Water (AASW), Circumpolar Deep Water (CDW), Modified Circumpolar Deep Water (MCDW), Shelf Water (SW), Modified Shelf Water (MSW), and Terra Nova Bay Ice Shelf Water (TISW). Contours show interpolated neutral density surfaces. Red arrows at upper left of panel (a) indicate stations that were occupied soon after each of the two major katabatic wind events.

3.2. The Drygalski Trough-Terra Nova Bay Transect

3.2.1. Sampling Conditions and Hydrography

On the southbound cruise leg, we sampled four locations along the Drygalski Trough, between the shelf break off Cape McCormick and the northeastern edge of the Terra Nova Bay basin (stations 1–4, Figure 2a). Another eight sites were sampled over an 8-day period (May 2–10, 2017) within the Terra Nova Bay polynya (stations 5–12, Figure 2a), during which we observed two intense katabatic events with sustained wind speeds >30 m s^{-1}, air temperatures < −20°C, and active formation of pancake ice and associated vertical mixing of the water column (Ackley et al., 2020; Thompson et al., 2020). In addition to the katabatic events, our sampling period in Terra Nova Bay was also impacted by strong to gale-force winds of ~15–20 m s^{-1} for several days. Figures 3a and 3b show quasi-meridional sections of temperature (T) and salinity (S), respectively, interpolated between the trace-metal CTD sampling stations 1–11 along the Drygalski Trough-Terra Nova Bay transect, with white contour lines showing interpolated neutral density (γ^n) surfaces (Jackett & McDougall, 1997).

Water masses identified from the hydrographic data in Figure 3 follow the classification of Orsi and Wiederwohl (2009), and include the cold, fresh Antarctic Surface Water (AASW, $\gamma^n < 28.0$ kg m^{-3}); the warm, salty Circumpolar Deep Water (CDW, $28.0 < \gamma^n < 28.27$ kg m^{-3}), which cools, freshens, and shoals as it intrudes southward from the shelf break to form Modified Circumpolar Deep Water (MCDW, $28.0 < \gamma^n < 28.27$ kg m^{-3}); and the cold, salty Shelf Water (SW, $\gamma^n > 28.27$ kg m^{-3}, potential temperature < -1.85°C), which mixes with MCDW to form Modified Shelf Water (MSW, $\gamma^n > 28.27$ kg m^{-3}, potential temperature > -1.85°C). In addition, the hydrographic data from stations 4 to11 in Terra Nova Bay clearly show intrusions of Terra Nova Bay Ice Shelf Water (TISW), which is formed through the interaction of the SW with the base of glacial ice and defined by potential temperatures less than −1.93°C (Budillon & Spezie, 2000; Yoon et al., 2020), within the SW.

A notable feature revealed by our hydrographic data is the large range in vertical mixing depths across the nearly isothermal waters of Terra Nova Bay, where surface mixed layers varied from less than 250 to ∼600 m depth over lateral distances less than 10 km (Figure 3a, at far left). These observations suggest that vertical mixing driven by katabatic winds and sea ice production was extending into the most dense SW ($\gamma^n > 28.7$ kg m^{-3}, $S > 34.7$), heralding the onset of deep convective overturn in the Terra Nova Bay polynya (Ackley et al., 2020; Thompson et al., 2020). The differences in the surface mixed layer depth between our stations are not clearly related to the timing of the two katabatic wind events, which preceded our sampling of stations 5 and 7 (indicated by red arrows in Figure 3a). Instead, these differences may reflect lateral heterogeneity in the formation of sea ice across the polynya, and/or Ekman transport of the upper water column driven by the strong westerly winds. Our data also delineate the resultant shoaling outflow of this highly saline SW from the Terra Nova Bay basin northward along the Drygalski Trough toward the shelf break (Figure 3a), from where these dense waters descend and contribute to the Antarctic Bottom Water (e.g., Budillon et al., 2011; Gordon et al., 2004).

3.2.2. Dissolved Trace Metals

Along the Drygalski Trough (stations 1–4, Figure 4a), the distribution of DFe is mostly characterized by low concentrations (∼0.2 nM or less) within the near-surface AASW and MCDW, and somewhat higher concentrations of ∼0.3–0.6 nM in the underlying MSW and SW. These concentrations are generally consistent with previous measurements of DFe in samples collected over the Ross Sea shelf during summer (e.g., Coale et al., 2005; Fitzwater et al., 2000; Gerringa et al., 2015; Hatta et al., 2017; Marsay et al., 2014, 2017; Sedwick et al., 2000, 2011), with the low AASW concentrations reflecting biological uptake during the preceding growing season. The DFe profiles from these stations also display slight, near-surface maxima ranging from ∼0.2 to ∼0.4 nM (Figure 5), as previously reported for the western Ross Sea (Sedwick et al., 2011). These features are possibly associated with the formation or melting of sea ice, which may concentrate or release dissolved iron species near the sea surface, respectively (Lannuzel et al., 2016); both of these physical processes were observed along the Drygalski Trough-Terra Nova Bay transect, with sea ice actively forming south of ∼74°S, and melting north of ∼74°S (Ackley et al., 2020). The inner-shelf stations along this transect (stations 3–11, Figure 4a) all show elevated DFe concentrations toward the seafloor, as has been observed over much of the Ross Sea shelf (Coale et al., 2005; Gerringa et al., 2015; Hatta et al., 2017; Marsay et al., 2014, 2017; Sedwick et al., 2011).

Figure 4b shows the DFe concentrations of samples collected along the Drygalski Trough-Terra Nova Bay transect in potential temperature-salinity space. All of the elevated DFe concentrations (>0.4 nM) are associated with dense SW or TISW (salinities > 34.6 and potential temperatures < -1.8°C), with the exception of the higher concentrations in CDW at station 1, and in AASW at station 2, the latter perhaps associated with melting sea ice. The DFe profiles from stations 3, 4, 5, and 7 show concentration maxima of ∼0.5–1 nM at various depths between 100 and 500 m (Figure 5), which may reflect advective inputs from nearshore waters or near-bottom waters over adjacent shallow banks, where DFe concentrations are typically elevated (e.g., Grotti et al., 2001; Marsay et al., 2014, 2017). In addition, the elevated near-surface DFe concentrations at station 5 may reflect processes associated with sea ice formation, as indicated by the excess xenon and krypton (which are excluded during sea ice formation) and deficit in helium (which is preferentially incorporated in sea ice) measured in surface samples collected from a nearby station using the ship's conventional CTD-rosette (Loose et al., 2022). Other potential sources of DFe at these depths are the remineralization of organic matter vertically exported from the preceding growing season (DeJong et al., 2017; Giordano et al., 2020), and glacial meltwaters (Annett et al., 2015; McGillicuddy et al., 2015), although with regard to glacial inputs we see no clear evidence that elevated DFe concentrations are associated with intrusions of TISW (Figure 5).

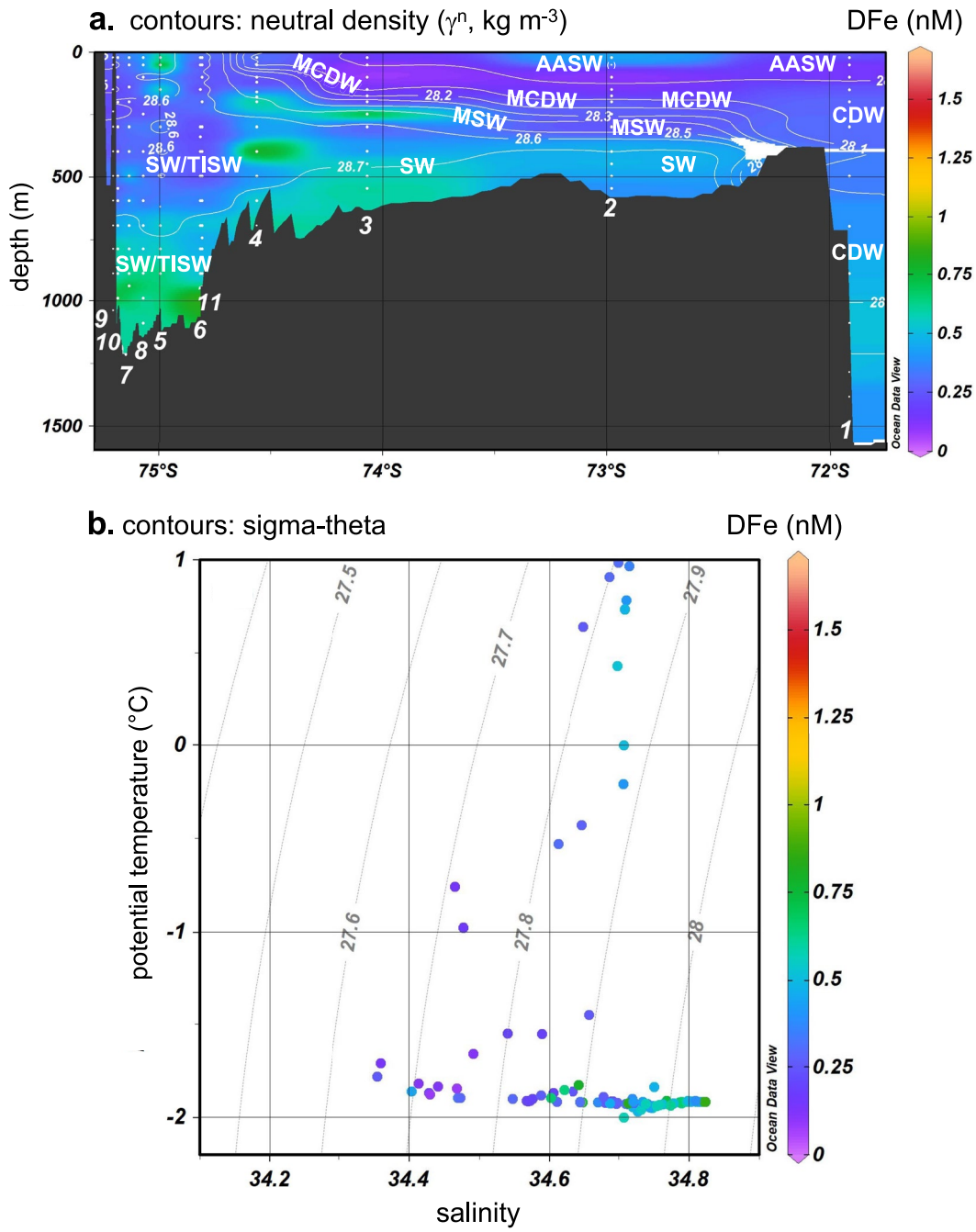

Figure 4. (a) Interpolated section of dissolved iron (DFe) concentration along the Drygalski Trough-Terra Nova Bay transect (stations 1–11); also shown are water masses (as for Figure 3) and interpolated neutral density surfaces. (b) DFe concentrations of samples from stations 1 to 11 in potential temperature-salinity space.

In some instances, our measurements of dissolved manganese (DMn) and zinc (DZn) may allow us to discriminate between DFe supplied from sediment sources (Jensen et al., 2020; Measures et al., 2013; Middag et al., 2012) versus remineralization of biogenic material (Coale et al., 2005; Croot et al., 2011; Vance et al., 2017). Along the Drygalski Trough-Terra Nova Bay transect, the contrasting geochemical behavior of these two trace metals is clearly demonstrated by our data from station 1, where DMn (a scavenged-type element) and DZn (a nutrient-type element) display the minimum and maximum concentrations, respectively, within the old, nutrient-rich CDW (Figures 6a and 6b). Further, reducing sediments are thought to be important sources of DMn in continental

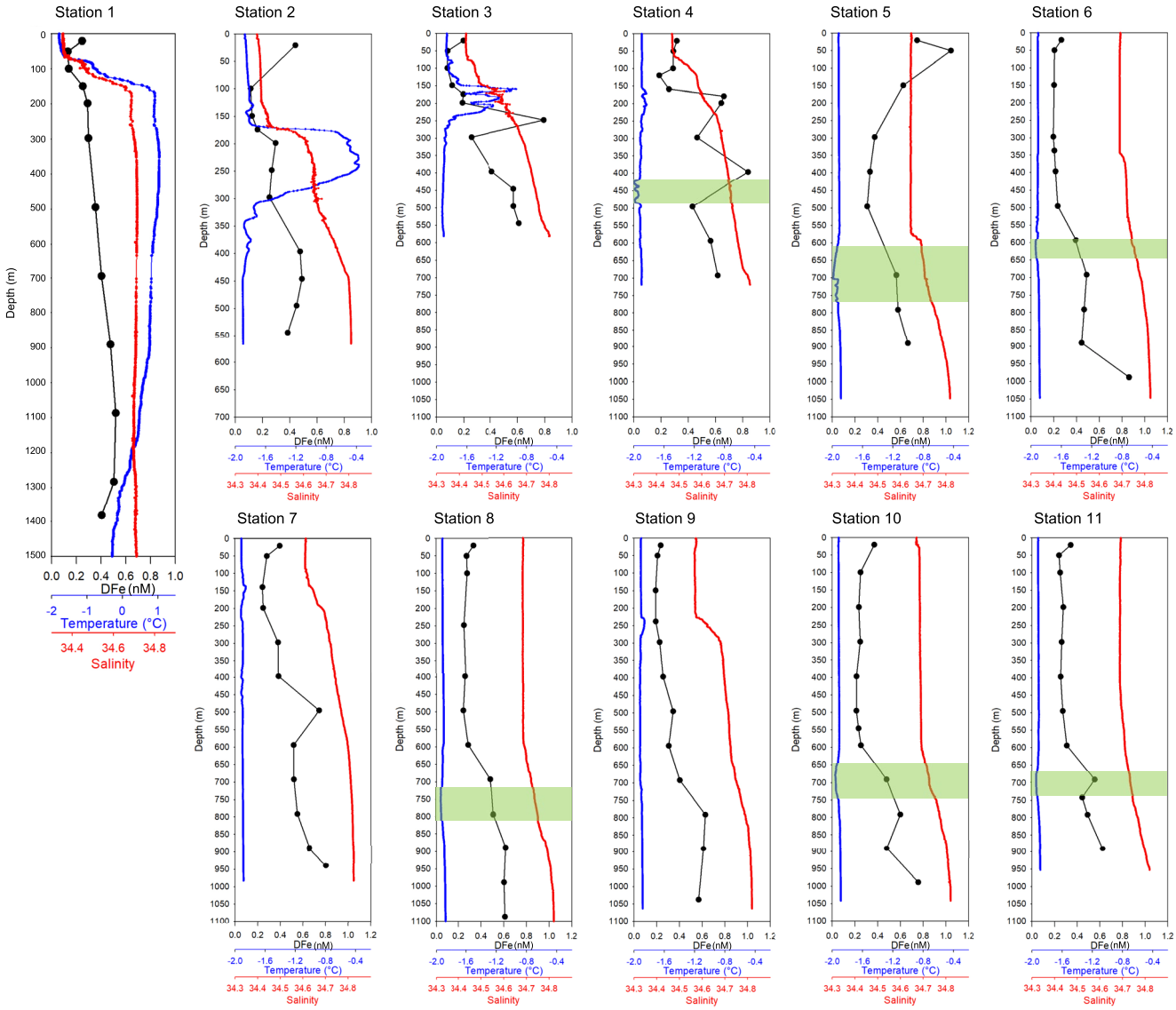

Figure 5. Vertical profiles of temperature, salinity, and dissolved iron (DFe) concentration along the Drygalski Trough-Terra Nova Bay transect (stations 1–11). Green shaded depth intervals indicate apparent intrusions of colder Terra Nova Bay Ice Shelf Water (TISW, potential temperature < −1.93°C). Station locations are shown in Figure 2a.

shelf waters (Heggie et al., 1987; Jensen et al., 2020; Measures et al., 2013). Over the inner shelf in Terra Nova Bay, isolated mid-depth DFe maxima at ~400 m at station 4 and ~500 m at station 7 (Figure 4a) may reflect plume-like, lateral inputs from sedimentary sources, based on similarly isolated maxima in DMn (Figure 6a), in contrast to the generally elevated concentrations of DZn below 250 m depth observed at both stations (Figure 6b). Conversely, the elevated DZn concentration associated with the DFe maxima at ~250 m depth at station 3 (Figures 4a and 6b) may indicate inputs from the remineralization of organic matter, perhaps associated with earlier biological production in the DZn-depleted upper water column at station 4.

At depths greater than 500 m, the broadly similar distributions of DFe and DMn across the section that includes stations 3–11 (Figures 4a and 6a) suggest that elevated DFe concentrations in the deep Terra Nova Bay basin are primarily derived from resuspended sediments and/or sediment pore fluids (Burdige & Christensen, 2022; Marsay et al., 2017; Measures et al., 2013; Sherrell et al., 2018), rather than from remineralization of biogenic material within the water column as inferred from elevated DZn concentrations. In contrast to DFe and DMn, which show pronounced enrichment toward the seafloor (Figures 4a and 6a), elevated DZn concentrations extend

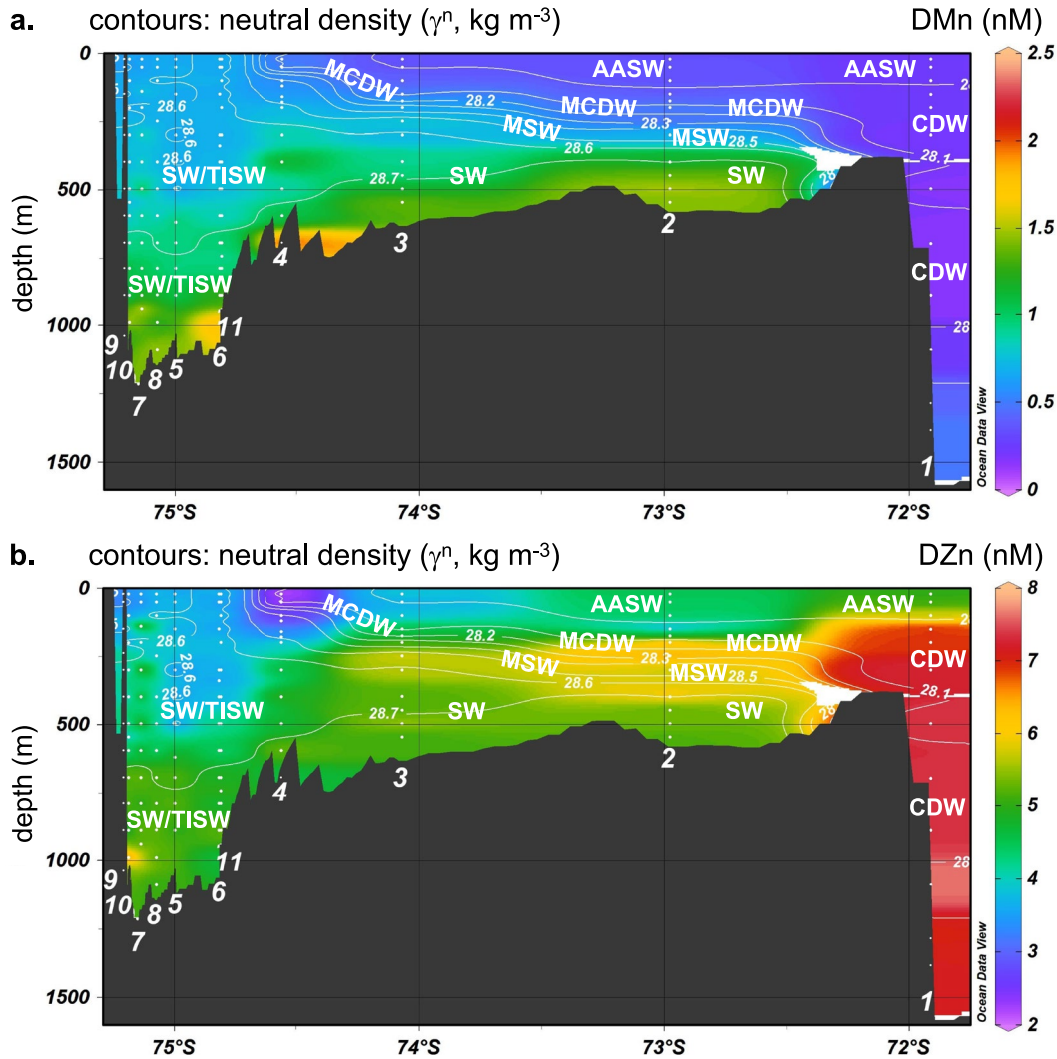

Figure 6. Interpolated sections of (a) dissolved manganese (DMn) concentration and (b) dissolved zinc (DZn) concentration along the Drygalski Trough-Terra Nova Bay transect (stations 1–11). Also shown are water masses (as for Figure 3) and neutral density surfaces.

to depths shallower than 500 m (Figure 6b), such that vertical mixing was likely supplying considerable amounts of DZn (but not DFe) to surface waters of Terra Nova Bay during our cruise period. However, it should also be noted that both DFe and DZn concentrations were elevated in some samples near the seafloor (e.g., see stations 4 and 10 in Figures 4a and 6b), which suggests that elevated DFe may also reflect inputs from remineralization of organic matter on the seafloor or within the benthic boundary layer. Interestingly, our data suggest that there may be a substantial loss of DFe, relative to DMn, as dense SW is transported northwards along the Drygalski Trough between stations 3 and 2. Whereas DMn concentrations were elevated within the highly saline SW at both of these stations (Figure 6a), elevated SW DFe concentrations were only observed at station 3; at station 2, SW DFe concentrations were similar to values measured in the CDW (Figure 4a). These observations imply that northwards export of SW might not constitute a major off-shelf flux of DFe in the western Ross Sea.

Oldham et al. (2021) have recently reported much higher concentrations of DMn in water column samples from the western Ross Sea compared to the values measured in our PIPERS samples and from previous studies that collected samples during austral spring and summer (Gerringa et al., 2020; Sedwick et al., 2000). For stations sampled in February–March 2018, including stations in Terra Nova Bay, Oldham et al. (2021) report an average concentration of 10 ± 14 nM for total dissolved manganese, which was comprised of varying proportions of Mn(II) and organically complexed Mn(III); they suggest that these relatively high DMn concentrations may

reflect the precipitation of dissolved Mn(III)-humic complexes upon acidification of filtered samples in previous studies. Such relatively high DMn concentrations are plausible, but are typically associated with nearshore waters on the Antarctic continental margins (e.g., Forsch et al., 2021; Grotti et al., 2001; Martin et al., 1990); we also note that Sedwick et al. (2000) report mean water-column DMn concentrations in the Ross Sea of 0.48 nM (spring 1994) and 0.39 nM (summer 1995) in filtered samples that had *not* been acidified before shipboard analysis. Further, Milne et al. (2010) reported no significant differences in the measured DMn concentrations of SAFe S1 and D2 reference seawater following UV irradiation, which would be expected to destroy organic ligands that complex Mn(III). However, given the importance of manganese as a geochemical tracer and essential micronutrient (Anderson, 2020; Browning et al., 2021), further work is warranted to resolve this large discrepancy in measured DMn concentrations in waters over the Ross Sea continental shelf.

3.2.3. Particulate Trace Metals

The distributions of particulate (>0.2 μm) iron (PFe), manganese (PMn), and aluminum (PAl) exhibit generally similar patterns along the Drygalski Trough-Terra Nova Bay transect (Figure 7), with the highest concentrations toward the seafloor and in the deep Terra Nova Bay basin. Consistent with previous studies, the concentrations of PFe in the upper water column are roughly an order of magnitude greater than DFe, with higher PFe concentrations observed over the inner shelf (Coale et al., 2005; Marsay et al., 2017; Sedwick et al., 2011). The elevated concentrations of PFe, PMn, and PAl near the seafloor are presumably associated with resuspended sediments and/or benthic nepheloid layers, which are thought to be dominated by lithogenic and authigenic phases on the Ross Sea shelf (Marsay et al., 2017). The similarity of the DFe distribution (Figure 4a) to those of PFe, PMn, and PAl (Figure 7) would then seem to support the idea that the elevated DFe concentrations within the dense SW are mainly derived from sediment pore fluids and/or release from suspended particles, as proposed by Marsay et al. (2017).

The particulate metal data also reveal a number of concentration anomalies at shallower depths in the water column. These include maxima in PFe, PMn, and PAl in the 600–800 m depth range centered at stations 5 and 7 (Figure 7). At station 5, these maxima appear to coincide with an intrusion of TISW although without a corresponding maxima in DFe (Figure 5), which may reflect inputs of relatively refractory lithogenic particles in glacial melt water (Krisch et al., 2021). There were also isolated PMn maxima at depths of 50 and 400 m (Figure 7b) and PAl maxima within the upper 200 m (Figure 7c), which are not readily explained. Of potential importance with regard to the off-shelf transport of iron are the elevated concentrations of both PFe and PMn within the deepest samples at station 2. Noting that the dense SW was enriched in DMn but not DFe at station 2, this suggests that DFe may be lost to the particulate phase as high salinity SW is transported north toward the shelf break, perhaps modulated by the limited availability of dissolved iron-binding ligands in SW (e.g., see Thuróczy et al., 2012).

3.3. Ross Ice Shelf Transect

3.3.1. Sampling Conditions and Hydrography

After completing sampling in Terra Nova Bay and an additional site southeast of Crary Bank (station 13, Figure 2), we sampled five stations that define a zonal transect across the Ross Ice Shelf polynya, immediately north of the Ross Ice Shelf (stations 14–18, Figure 2b). This 2-day sampling period (May 16–17, 2017) was characterized by moderate off-ice-shelf winds accompanied by the formation of frazil, nilas, and young gray sea ice. Figures 8a and 8b show quasi-zonal sections of salinity and temperature interpolated between trace-metal CTD sampling stations 14 through 18. Surface mixed layers were relatively shallow, ranging from a maximum of ∼300 m in the west to less than 100 m in the east, suggesting that the less extreme weather we experienced was more typical of this area before sampling, rather than the intense katabatic wind events that we observed impacting the Terra Nova Bay region. The main water masses identified from the hydrographic data in Figure 8 again follow the classification of Orsi and Wiederwohl (2009), and include MCDW ($28.0 < \gamma^n < 28.27$ kg m^{-3}, $T < 0$°C) over the upper water column at stations 14, 15, and 18; AASW ($\gamma^n < 28.0$ kg m^{-3}), which was present at stations 16 and 17; and SW ($\gamma^n > 28.27$ kg m^{-3}, potential temperature < -1.85°C), which was observed below depths ranging from ∼100 to ∼400 m. Also observed was an intrusion of Ice Shelf Water (ISW) centered in the 450–500 m depth range at stations 16 and 17 (Figure 8b), as indicated by potential temperatures below −1.95°C,

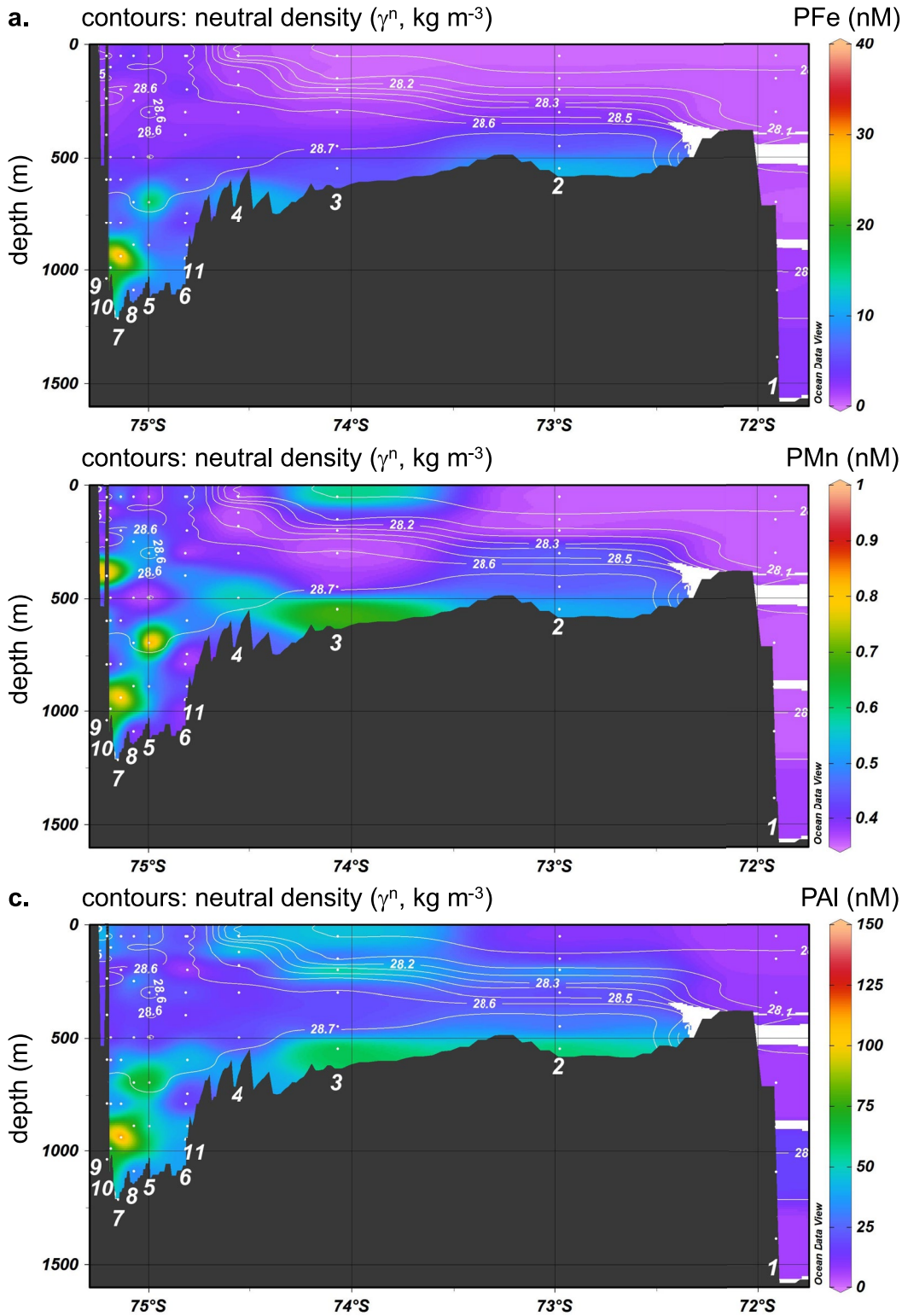

Figure 7. Interpolated sections of (a) particulate iron (PFe) concentration, (b) particulate manganese (PMn) concentration, and (c) particulate aluminum (PAl) concentration along the Drygalski Trough-Terra Nova Bay transect (stations 1–11). Also shown are interpolated neutral density surfaces.

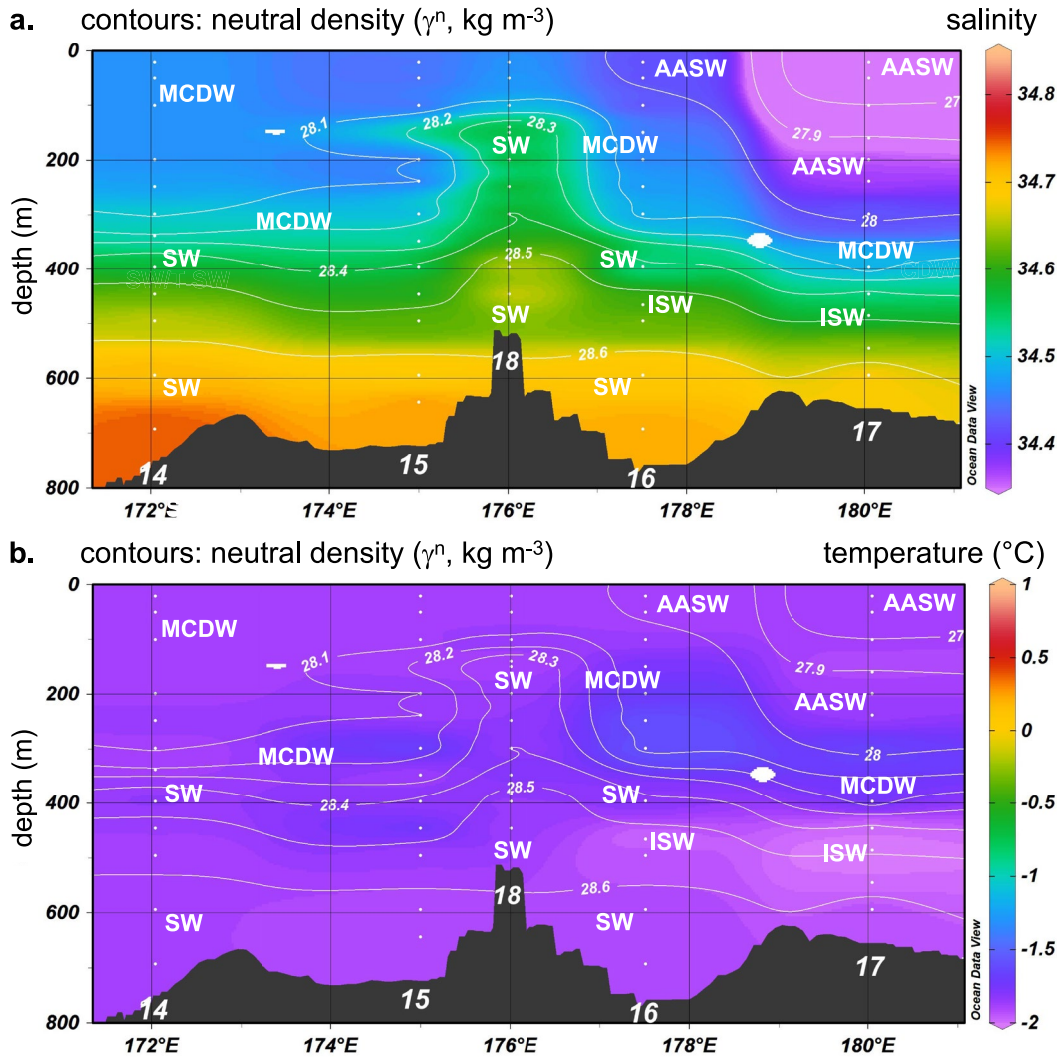

Figure 8. Interpolated sections of (a) salinity and (b) temperature along the Ross Ice Shelf transect (stations 14–18), showing Antarctic Surface Water (AASW), Modified Circumpolar Deep Water (MCDW), Shelf Water (SW), and Ice Shelf Water (ISW). Contours show interpolated neutral density surfaces.

and by saturation anomalies in helium and neon (which are enriched in glacial meltwaters) in samples collected at a nearby CTD station (Loose et al., 2022). The ISW is thought to be formed through the interaction of SW with the glacial ice shelf, and has been previously observed north of the Ross Ice Shelf near the 180° meridian (Jacobs & Giulivi, 1985; Orsi & Wiederwohl, 2009; Smethie & Jacobs, 2005). Saturation anomalies in dissolved helium and neon in samples collected along the Ross Ice Shelf section suggest glacial meltwater contributions of up to ~1% (Loose et al., 2022).

3.3.2. Dissolved Trace Metals

The vertical distribution of DFe along the Ross Ice Shelf transect (Figures 9 and 10) was remarkably similar to that reported for samples collected from this area in mid to late summer, with DFe concentrations of ~0.1–0.2 nM over the upper 300–400 m of the water column (Gerringa et al., 2015; Marsay et al., 2017; Sedwick et al., 2011). These low DFe concentrations in the upper water column presumably reflect the cumulative imprint of the biological uptake and scavenging that accompany phytoplankton blooms and associated particle export in this region during the austral summer and fall (Cochran et al., 2000; Smith et al., 2012). At depths greater than 350–400 m, well below the extent of the surface mixed layer, DFe concentrations increase toward the seafloor. The highest DFe concentrations were measured in the deepest samples collected from stations 15 and 18, located

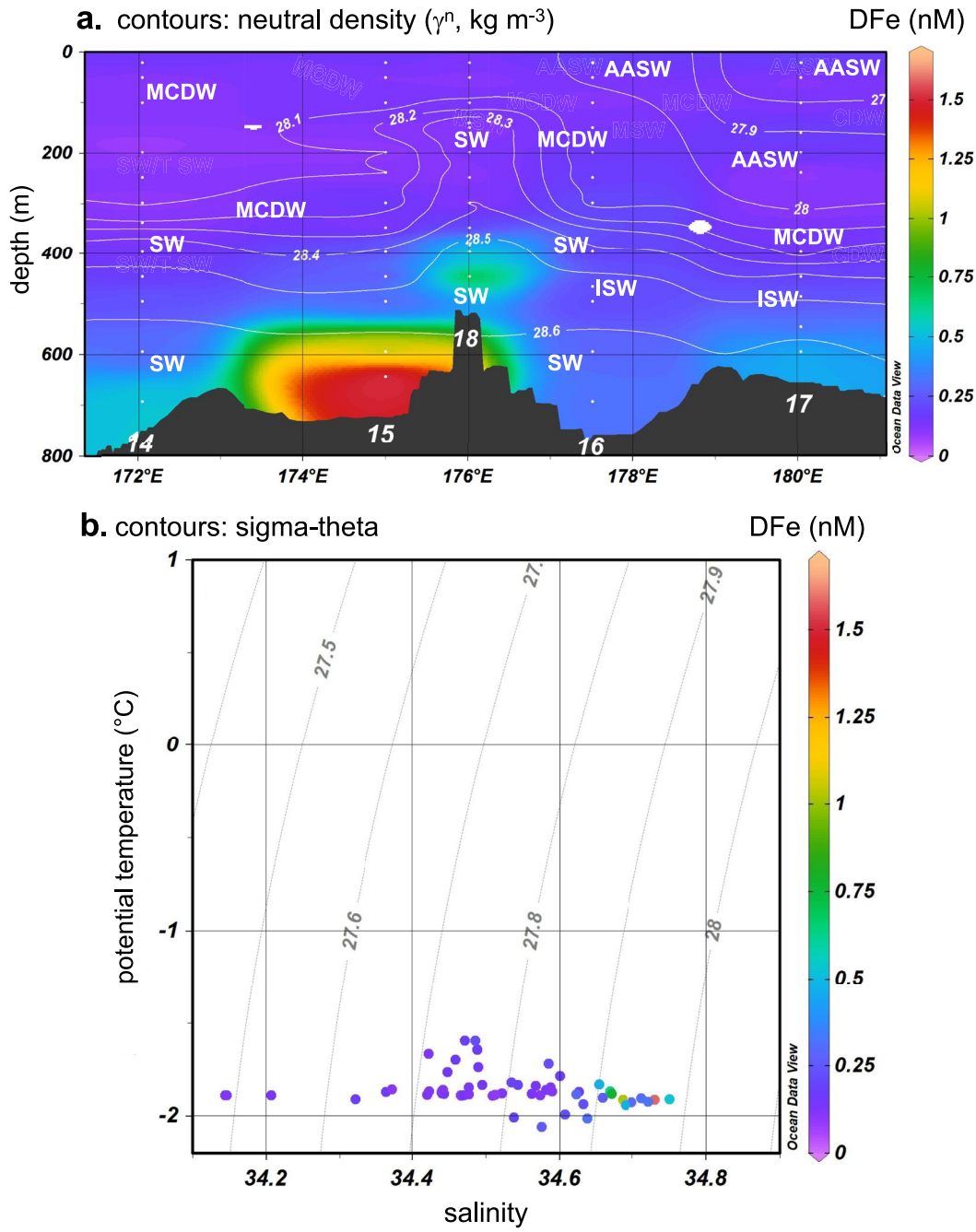

Figure 9. (a) Interpolated section of dissolved iron (DFe) concentration along the Ross Ice Shelf transect (stations 14–18); also shown are water masses (as for Figure 8) and interpolated neutral density surfaces. Color scales are the same as used in Figure 4a. (b) DFe concentrations of samples from stations 14 to 18 in potential temperature-salinity space.

to the south of Ross Bank (Figures 9a and 10), and from station 13, which was located to the southeast of Crary Bank (Figure 10).

As observed for the Terra Nova Bay stations, the elevated DFe concentrations along the Ross Ice Shelf transect were associated with the highly saline SW ($S > 34.6$, Figure 9b). Within these denser waters, the distribution of DMn (Figure 11a) shows concentration maxima that closely resemble those for DFe, whereas DZn concentrations (Figure 11b) increase more uniformly with depth. This again suggests that elevated DFe concentrations near the seafloor reflect inputs from resuspended sediments and/or sediment pore fluids, rather than remineralization of

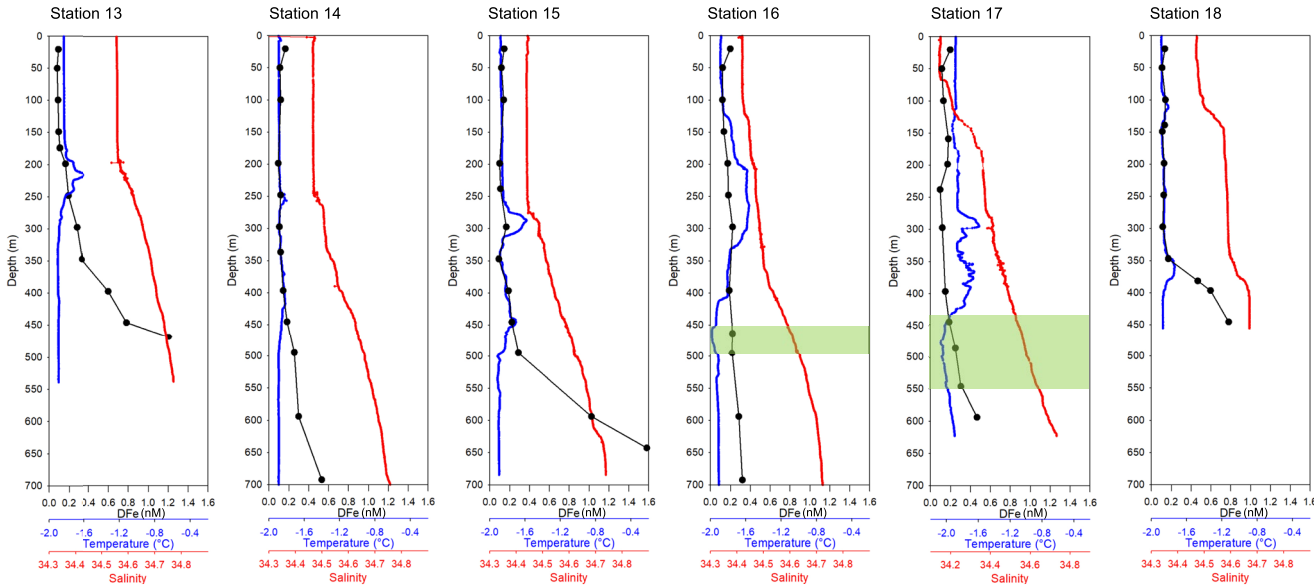

Figure 10. Vertical profiles of temperature, salinity, and dissolved iron (DFe) concentration along the Ross Ice Shelf transect (stations 14–18); also shown are profiles from station 13, located to the southeast of Crary Bank (see Figure 2a). Green shaded depth intervals indicate apparent intrusions of colder Ice Shelf Water (ISW, potential temperature < -1.95°C). Station locations are shown in Figure 2b.

organic matter, although the latter process may contribute to the elevated DFe concentrations at depth, particularly within the benthic boundary layer. In this regard, we note that DFe and DMn concentrations were not clearly elevated at depth at station 16. At this station, our deepest sample was collected ∼80 m above the seafloor, which was perhaps shallower than the benthic nepheloid layer; unfortunately, we lack transmissometer data to verify this possibility. Alternately, the low DFe and DMn concentrations near the seafloor at station 16 may be an advective feature reflecting the northward transport of deep waters to the east of Ross Bank, as we discuss further in Section 3.4. Neither DFe, DMn nor DZn showed elevated concentrations within the very cold ISW that was sampled at stations 16 and 17 (Figures 9a, 10, and 11), consistent with previous data suggesting that DFe concentrations are not substantially elevated within that water mass (Marsay et al., 2017).

3.3.3. Particulate Trace Metals

The distributions of PFe, PMn, and PAl along the Ross Ice Shelf transect are shown in Figure 12 (no particulate samples were collected from station 18). At the western end of the section, stations 14 and 15 show elevated concentrations of PFe, PMn, and PAl near the seafloor, consistent with the suggestion that the elevated DFe concentrations here are derived from resuspended sediments. Further, at station 16, where DFe was not elevated in the deepest sample, PFe, PMn, and PAl concentrations were only slightly elevated at depth (no particulates were collected from the two deepest samples at station 17). Whereas elevated PFe concentrations (>5 nM) were only observed toward the seafloor, less pronounced maxima in PMn and PAl concentrations were also observed at shallower depths in the water column (Figures 12b and 12c). The PMn maxima at depths of 200–400 m (Figure 12b) may reflect particles carried from shallow Ross Bank, as might the PAl maxima at 400 m depth (Figure 12c). The elevated PAl concentrations in the upper 200 m of the water column (Figure 12c) are perhaps associated with biogenic silica produced by late-season diatom blooms, given that aluminum is thought to be incorporated into diatom frustules (Gehlen et al., 2002); we note that similarly elevated PAl concentrations were observed in the upper water column along the Drygalski Trough-Terra Nova Bay transect (Figure 7c).

3.4. A Model-Data Comparison: Implications for the Vertical Resupply of DFe

Given the importance of iron in regulating primary production on the Antarctic margins and adjacent Southern Ocean, a number of studies have used numerical modeling to examine the sources and transport of DFe on the Antarctic continental shelf, and their propensity for future change (e.g., Arrigo et al., 2003; Death et al., 2014; Dinniman et al., 2020; Lancelot et al., 2009; Laufkoetter et al., 2018; Mack et al., 2017; Person

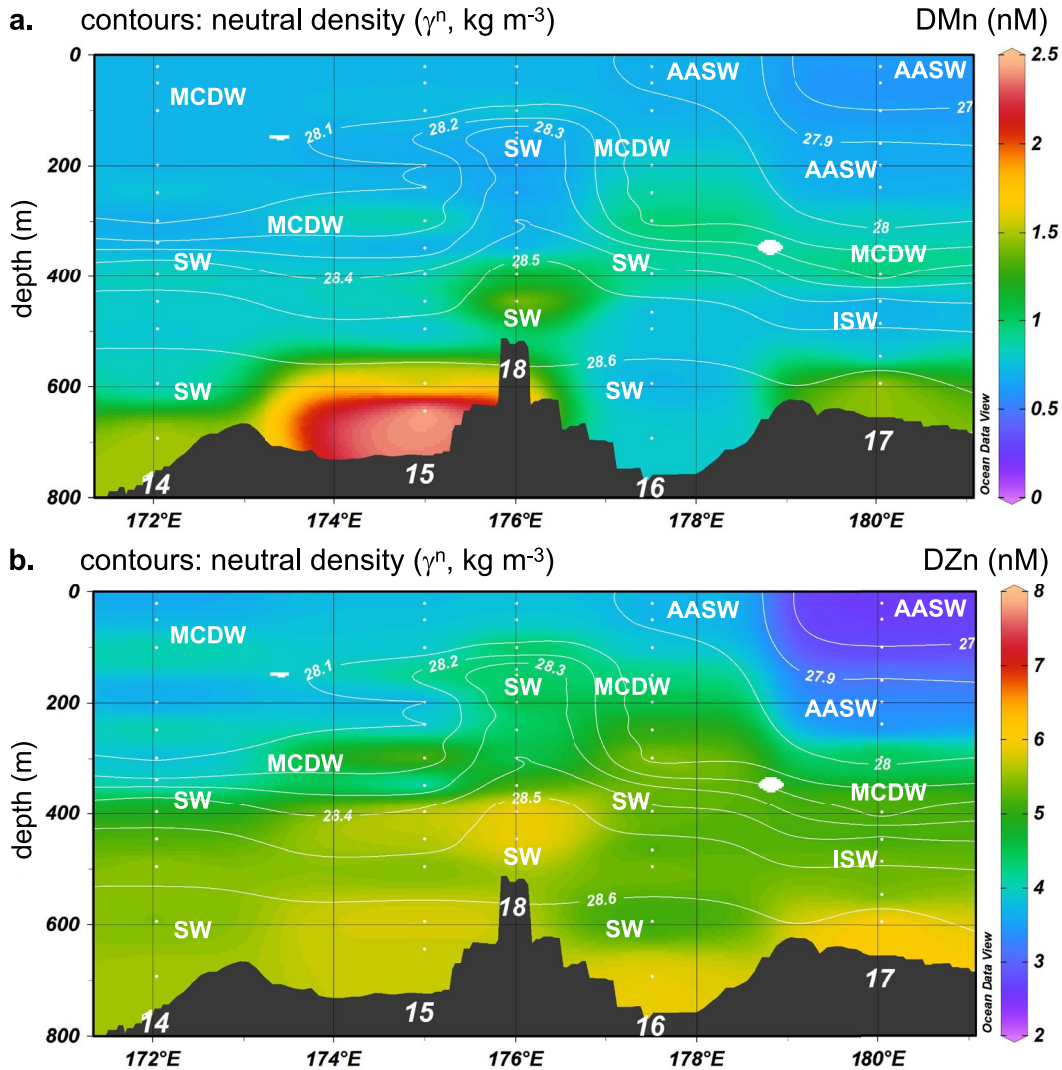

Figure 11. Interpolated sections of (a) dissolved manganese (DMn) concentration and (b) dissolved zinc (DZn) concentration along the Ross Ice Shelf transect (stations 14–18). Also shown are water masses (as for Figure 8) and neutral density surfaces. Color scales are the same as used in Figure 6.

et al., 2019, 2020, 2021; St-Laurent et al., 2017, 2019; Tagliabue & Arrigo, 2005, 2006; Wang et al., 2014). Comparisons of model solutions with field data are crucial in assessing the skill of such numerical models and thus the veracity of associated future projections. Although there is an increasing body of data available for the distribution of DFe over the Antarctic shelf, those data are largely confined to the austral summer months, when field campaigns are mounted. In this context, our PIPERS data are an important resource, in that they allow model-data comparisons for DFe in the Ross Sea under the different physical and biological conditions of the austral fall.

Here we present one such comparison, for model solutions from the recent study by Dinniman et al. (2020), which uses an ocean/sea-ice/ice-shelf model of the Southern Ocean to examine the mechanisms that supply DFe to surface waters over the Antarctic continental shelf. The model is an implementation of the Regional Ocean Modeling System with a 5-km horizontal resolution that includes a dynamic sea-ice model, and the mechanical and thermodynamic interactions between floating ice shelves and the ocean waters beneath. The model introduces DFe as conservative, independent tracers supplied from four sources—sediments, CDW, sea ice melt, and ice shelf melt—using assumed source concentrations and idealized scavenging and summer biological uptake (complete details are provided by Dinniman et al., 2020); the model does not consider iron-binding ligands nor

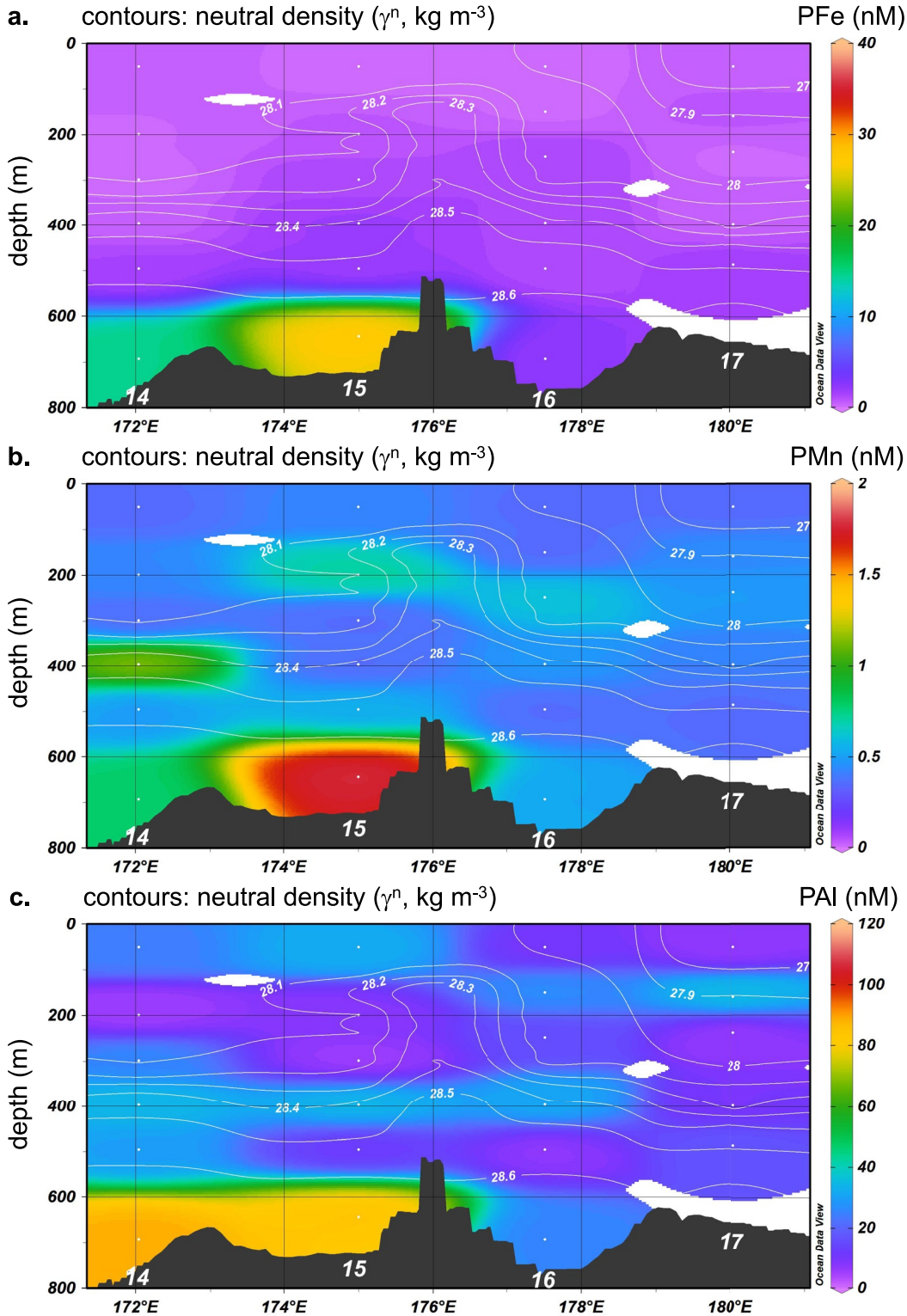

Figure 12. Interpolated sections of (a) particulate iron (PFe) concentration, (b) particulate manganese (PMn) concentration, and (c) particulate aluminum (PAl) concentration along the Ross Ice Shelf transect (stations 14–18). Also shown are interpolated neutral density surfaces. Color scales are the same as used in Figure 7.

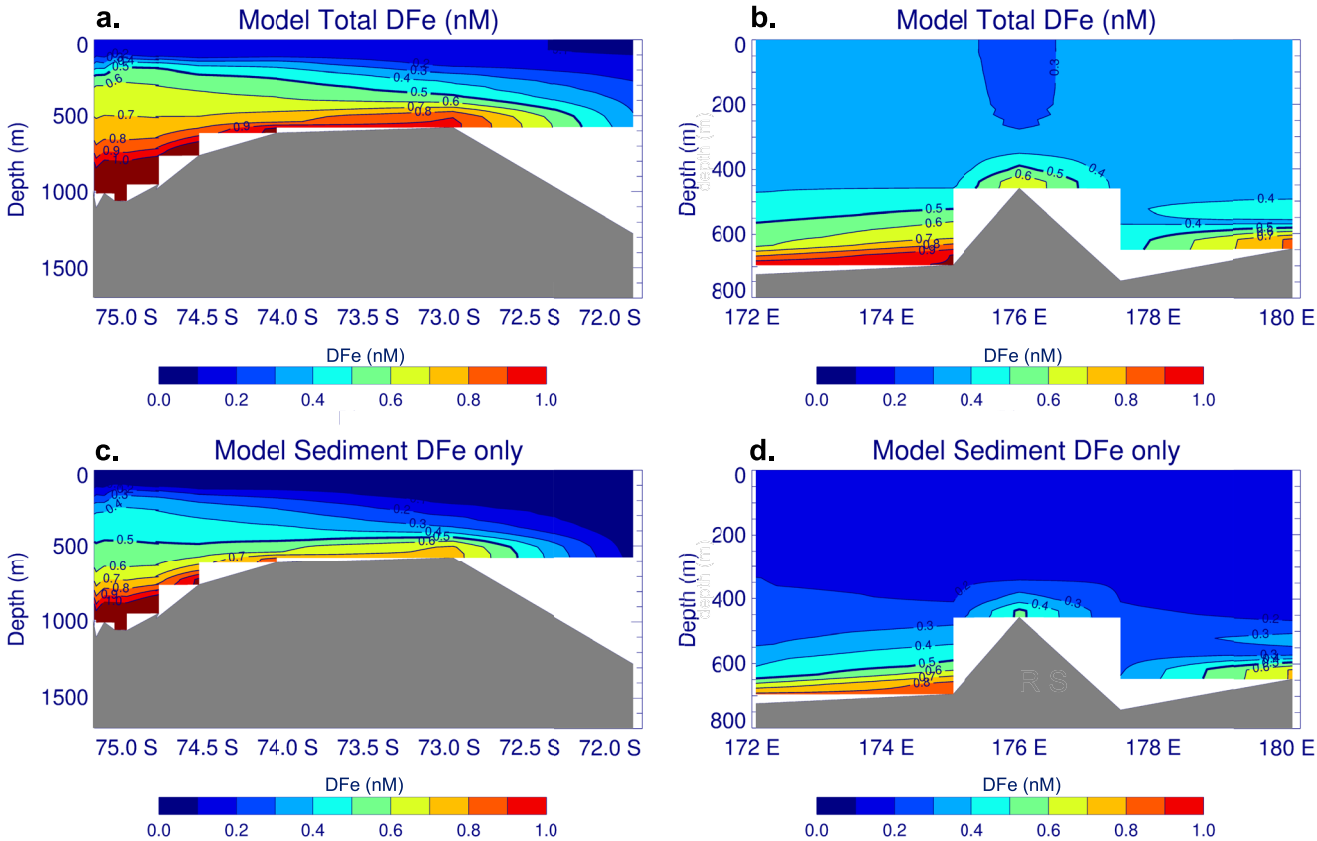

Figure 13. Mid-May solutions from the model of Dinniman et al. (2020) for DFe concentrations derived from all sources along (a) Drygalski Trough-Terra Nova Bay transect, and (b) Ross Ice Shelf transect; and for sediment-derived DFe concentrations along (c) Drygalski Trough-Terra Nova Bay transect, and (d) Ross Ice Shelf transect.

colloidal iron species, both of which may play important roles in the removal of DFe from seawater (e.g., Kunde et al., 2019; Thuróczy et al., 2012). For the PIPERS study region in the western Ross Sea, the model solutions suggest that DFe supply is dominated by sediments, followed by CDW and (during summer months) sea ice melt.

Figure 13 presents the model solutions for DFe derived from all sources (upper panels) and sediment sources (lower panels) along the Drygalski Trough-Terra Nova Bay transect (left panels) and the Ross Ice Shelf transect (right panels), for model day 4150, which corresponds to mid-May in model-forcing year 2010. A comparison with the interpolated DFe sections in Figures 4a and 9a reveals reasonable qualitative agreement between the model solutions and observations, with the modeled sediment-derived DFe concentrations most closely resembling our data. The model solutions for the Drygalski Trough-Terra Nova Bay transect show elevated DFe concentrations of 0.5–0.7 nM at depths shallower than our observations, suggesting excessive vertical mixing in the modeled Terra Nova Bay polynya, as well as higher DFe concentrations at depth on the outer shelf (compare with Figure 4a). These differences may reflect both the unrealistically conservative behavior of the sediment-derived DFe tracer, and perhaps the late onset of convective mixing during fall 2017, relative to the climatological mean (see Section 3.1). Quantitatively, the interpolated average modeled DFe concentration for all stations and depths along the Drygalski Trough-Terra Nova Bay transect was 0.60 ± 0.38 nM, versus an average of 0.39 ± 0.19 nM for the observations. The Pearson and Spearman's correlation coefficients for the interpolated modeled versus observed DFe concentrations along this transect were 0.58 and 0.61, respectively, and are significantly different from zero at the 0.1% significance level.

The model is more successful in simulating DFe concentrations along the Ross Ice Shelf transect, including the higher values at depth to the west of Ross Bank, with the modeled sediment-derived DFe concentrations again appearing to be more consistent with our data (compare with Figure 9a). The interpolated average modeled DFe concentration for all stations and depths along the Ross Ice Shelf transect was 0.38 ± 0.12 nM, versus an average

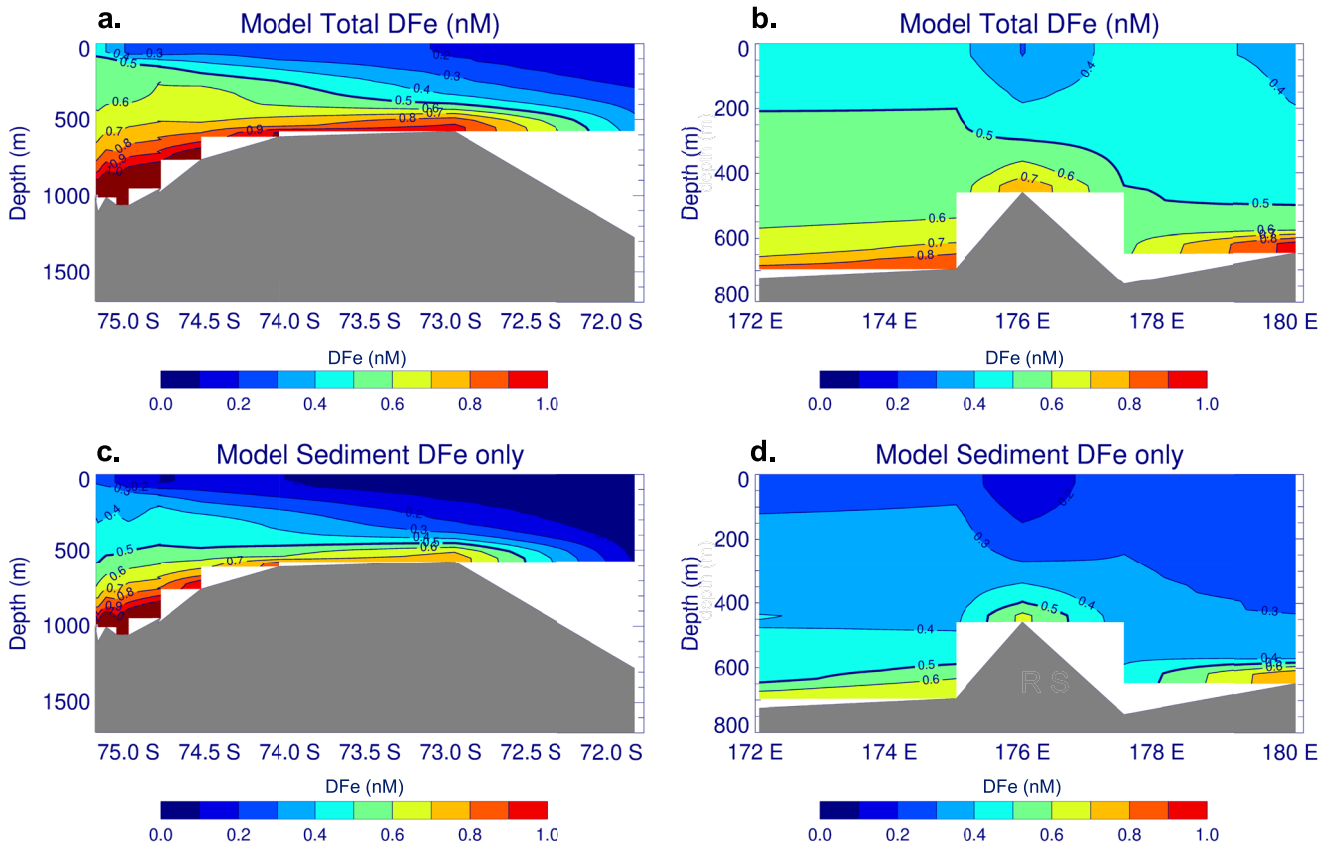

Figure 14. Late-November (before biological uptake) solutions from the model of Dinniman et al. (2020) for DFe concentrations derived from all sources along (a) Drygalski Trough-Terra Nova Bay transect, and (b) Ross Ice Shelf transect; and for sediment-derived DFe concentrations along (c) Drygalski Trough-Terra Nova Bay transect, and (d) Ross Ice Shelf transect.

of 0.21 ± 0.17 nM for the observations. The Pearson and Spearman's correlation coefficients for the interpolated modeled versus observed DFe concentrations along this transect were greater, at 0.82 and 0.72, respectively, and are again significantly different from zero at the 0.1% significance level. We note that the apparent zonal asymmetry in DFe concentrations across Ross Bank may be an advective feature, as the model simulations suggest that deep waters to the east of Ross Bank are carried northwards from beneath the Ross Ice Shelf, where sedimentary DFe sources are less important than on the open continental shelf. Previous field observations from this region are consistent with such circulation (e.g., Smethie & Jacobs, 2005).

Given the success of the model in simulating the broad-scale features of the PIPERS data set, it may be instructive to examine model solutions for DFe in austral spring, after winter mixing but prior to substantial biological uptake. Figure 14 shows those model solutions for DFe along the Drygalski Trough-Terra Nova Bay transect (left panels) and Ross Ice Shelf transect (right panels) for model day 4340, in late November. The simulations suggest that the concentrations of sediment-derived DFe exceed ~0.3 nM within the upper 100 m of the water column in our study areas, at least over the inner shelf, consistent with the limited DFe data reported for the Ross Sea from early spring (Coale et al., 2005; Fitzwater et al., 2000; Sedwick et al., 2000). These model results suggest that much of the seasonal vertical resupply of DFe over the Ross Sea shelf occurs during the mid-late winter months (after the April–May period of the PIPERS cruise), in accord with hydrographic data collected from CTD casts and moorings in Terra Nova Bay between 1995 and 2017 (Manzella et al., 1999; Rusciano et al., 2013; Yoon et al., 2020), from profiling floats north of the Ross Ice Shelf during 2014, 2015, and 2016 (Porter et al., 2019), and from instrumented seals on the inner-mid Ross Sea shelf during 2010, 2011, and 2012 (Piñones et al., 2019). This and the contrast between our observations from Terra Nova Bay, where sea ice formation was vigorous, and the RISP, where sea ice formation was much less intense, imply that the winter vertical resupply of DFe over the Ross Sea shelf may be particularly sensitive to the timing and extent of sea ice production in coastal polynyas.

4. Concluding Remarks

These first data on the distribution of DFe in the southwestern Ross Sea in late fall capture the onset of convective overturn in Terra Nova Bay, where intense katabatic wind events were driving vertical mixing into the iron-rich, highly saline SW. Based on our observations and numerical model simulations, it appears that the vertical resupply of DFe to surface waters in Terra Nova Bay, which likely sets the "winter reserve" of DFe for the subsequent growing season, progresses rapidly during the winter months following the late-fall cruise period. Our data document the lateral spread of the dense SW northward along the Drygalski Trough, although on the outer shelf these waters contained surprisingly low DFe concentrations, suggesting that DFe may be lost from the Terra Nova Bay SW as it is transported north toward the shelf break. Our results also reveal localized, near-surface DFe maxima that may be associated with the formation, transport, and melting of sea ice along the Drygalski Trough-Terra Nova Bay transect, and mid-depth concentration maxima that might reflect lateral transport from nearshore waters or adjacent banks. Within Terra Nova Bay, intrusions of cold TISW do not appear to carry substantially elevated DFe concentrations, relative to the SW, implying that glacial ice melt may not provide a major source of DFe in this region.

In contrast to the Terra Nova Bay polynya, the data from stations along the Ross Ice Shelf indicate that there had been limited vertical mixing before our PIPERS cruise observations. At these stations, surface mixed layers remained much shallower than the depths where elevated DFe concentrations were measured (>350–400 m), such that DFe concentrations over the upper 300 m were similar to the low values reported for samples collected from this region during summer (~0.1–0.2 nM). Together with numerical modeling results, which showed good skill in simulating the PIPERS DFe distributions, our data suggest that the vertical resupply of DFe to surface waters of the Ross Ice Shelf polynya occurs later in the winter months, relative to the Terra Nova Bay polynya. As such, both field observations and sample collections during the winter-spring period are required to document the impact of convective overturn on DFe over the Ross Sea shelf, and thereby assess the importance of this process in supplying iron to surface waters during the growing season. Also, consistent with our observations from Terra Nova Bay, an intrusion of very cold ISW along the Ross Ice Shelf transect did not exhibit elevated DFe concentrations. Finally, the water column distributions of dissolved manganese and zinc in both Terra Nova Bay and the RISP, and the concentrations of particulate iron, manganese, and aluminum, are consistent with the idea that resuspended sediments and/or sediment pore fluids provide the major sources of the elevated DFe concentrations that we observed in the deep, highly saline SW. Recently reported analyses of labile iron oxides in Antarctic Peninsula shelf sediments and micromolar concentrations of dissolved iron in associated sediment pore fluids (Burdige & Christensen, 2022) provide support for the importance of such sedimentary sources on the Ross Sea shelf.

An important implication from our field observations and the related numerical model simulations is that most of the vertical resupply of DFe over the Ross Sea shelf occurs after May, during the mid-late winter-season (~June–September), and that this process is strongly dependent on the timing and extent of sea ice production during that period. If so, then the documented recent declines in annual sea ice extent (Parkinson, 2019) and long-term freshening and warming (Jacobs et al., 2022) over the Ross Sea shelf might be expected to decrease the amount of DFe that is available to support phytoplankton growth, leading to recent and perhaps ongoing decreases in primary production over this sector of the Antarctic margin.

Acknowledgments
The authors gratefully acknowledge the contributions of the entire PIPERS science team, the officers and crew of RVIB *Nathaniel B. Palmer*, and the Antarctic Support Contractor personnel. The authors also thank Susann Henkel and two anonymous reviewers, whose comments greatly improved the manuscript. This study was supported by U.S. National Science Foundation (NSF) awards 1543483 to PNS, NSF 1341717 and NASA Grant 80NSSC19M0194 to SFA, NSF 1341606 and 1440435 to SES, and NSF 1643652 to MSD; JAR and NJB were funded by NOAA-PMEL Earth Oceans Interactions Program through the University of Washington Cooperative Institute for Climate, Ocean and Ecosystem studies. This is PMEL publication number 5391 and CICOES publication number 2022-1212.

Data Availability Statement

All of the data discussed here, along with associated metadata, are available from the U.S. National Science Foundation's Biological and Chemical Oceanography Data Management Office at: https://www.bco-dmo.org/dataset/856009.

References

Ackley, S. F., Stammerjohn, S., Maksym, T., Smith, M., Cassano, J., Guest, P., et al. (2020). Sea-ice production and air/ice/ocean/biogeochemistry interactions in the Ross Sea during the PIPERS 2017 autumn field campaign. *Annals of Glaciology*, *61*(82), 181–195. https://doi.org/10.1017/aog.2020.31

Anderson, R. F. (2020). GEOTRACES: Accelerating research on the marine biogeochemical cycles of trace elements and their isotopes. *Annual Review of Marine Science*, *12*, 49–85. https://doi.org/10.1146/annurev-marine-010318-095123

Annett, A. L., Skiba, M., Henley, S. F., Venables, H. J., Meredith, M. P., Statham, P. J., & Ganeshram, R. S. (2015). Comparative roles of upwelling and glacial iron sources in Ryder Bay, coastal western Antarctic Peninsula. *Marine Chemistry*, *176*, 21–33. https://doi.org/10.1016/j.marchem.2015.06.017

Arrigo, K. R., van Dijken, G. L., & Bushinsky, S. (2008). Primary production in the Southern Ocean, 1997–2006. *Journal of Geophysical Research*, *113*, C08004. https://doi.org/10.1029/2007JC004551

Arrigo, K. R., van Dijken, G. L., & Long, M. (2008b). Coastal Southern Ocean: A strong anthropogenic CO_2 sink. *Geophysical Research Letters*, *35*, L21602. https://doi.org/10.1029/2008GL035624

Arrigo, K. R., van Dijken, G. L., & Strong, A. L. (2015). Environmental controls of marine productivity hot spots around Antarctica. *Journal of Geophysical Research: Oceans*, *120*(8), 5545–5565. https://doi.org/10.1002/2015jc010888

Arrigo, K. R., Worthen, D. L., & Robinson, D. H. (2003). A coupled ocean-ecosystem model of the Ross Sea: 2. Iron regulation of phytoplankton taxonomic variability and primary production. *Journal of Geophysical Research*, *108*(C7), 3231. https://doi.org/10.1029/2001JC000856

Boyd, P. W. (2002). Environmental factors controlling phytoplankton processes in the Southern Ocean. *Journal of Phycology*, *38*(5), 844–861. https://doi.org/10.1046/j.1529-8817.2002.t01-1-01203.x

Boyd, P. W., Strzepek, R., Fu, F., & Hutchins, D. A. (2010). Environmental control of open-ocean phytoplankton groups: Now and in the future. *Limnology & Oceanography*, *55*(3), 1353–1376. https://doi.org/10.4319/lo.2010.55.3.1353

Browning, T. J., Achterberg, E. P., Engel, A., & Mawji, E. (2021). Manganese co-limitation of phytoplankton growth and major nutrient drawdown in the Southern Ocean. *Nature Communications*, *12*(1), 1–9. https://doi.org/10.1038/s41467-021-21122-6

Buck, N. J., Barrett, P. M., Morton, P. L., Landing, W. M., & Resing, J. A. (2021). Energy dispersive X-ray fluorescence methodology and analysis of suspended particulate matter in seawater for trace element compositions and an intercomparison with high-resolution inductively coupled plasma-mass spectrometry. *Limnology and Oceanography: Methods*, *19*(6), 401–415.

Budillon, G., Castagno, P., Aliani, S., Spezie, G., & Padman, L. (2011). Thermohaline variability and Antarctic bottom water formation at the Ross Sea shelf break. *Deep Sea Research Part I: Oceanographic Research Papers*, *58*(10), 1002–1018.

Budillon, G., & Spezie, G. (2000). Thermohaline structure and variability in the Terra Nova Bay polynya, Ross Sea. *Antarctic Science*, *12*(4), 493–508.

Burdige, D. J., & Christensen, J. P. (2022). Iron biogeochemistry in sediments on the western continental shelf of the Antarctic Peninsula. *Geochimica et Cosmochimica Acta*, *326*, 288–312.

Coale, K. H., Gordon, R. M., & Wang, X. (2005). The distribution and behavior of dissolved and particulate iron and zinc in the Ross Sea and Antarctic circumpolar current along 170 W. *Deep Sea Research Part I: Oceanographic Research Papers*, *52*(2), 295–318.

Coale, K. H., Johnson, K. S., Chavez, F. P., Buesseler, K. O., Barber, R. T., Brzezinski, M. A., et al. (2004). Southern Ocean iron enrichment experiment: Carbon cycling in high-and low-Si waters. *Science*, *304*(5669), 408–414.

Coale, K. H., Wang, X., Tanner, S. J., & Johnson, K. S. (2003). Phytoplankton growth and biological response to iron and zinc addition in the Ross Sea and Antarctic Circumpolar Current along 170°W. *Deep Sea Research Part II: Topical Studies in Oceanography*, *50*(3–4), 635–653.

Cochran, J. K., Buesseler, K. O., Bacon, M. P., Wang, H. W., Hirschberg, D. J., Ball, L., et al. (2000). Short-lived thorium isotopes (^{234}Th, ^{228}Th) as indicators of POC export and particle cycling in the Ross Sea, Southern Ocean. *Deep Sea Research Part II: Topical Studies in Oceanography*, *47*(15–16), 3451–3490.

Comiso, J. C., Kwok, R., Martin, S., & Gordon, A. L. (2011). Variability and trends in sea ice extent and ice production in the Ross Sea. *Journal of Geophysical Research*, *116*(C4), C04021.

Croot, P. L., Baars, O., & Streu, P. (2011). The distribution of dissolved zinc in the Atlantic sector of the Southern Ocean. *Deep Sea Research Part II: Topical Studies in Oceanography*, *58*(25–26), 2707–2719.

Cutter, G., Casciotti, K., Croot, P., Geibert, W., Heimbürger, L.-E., Lohan, M., et al. (2017). *Sampling and sample-handling protocols for GEOTRACES cruises, version 3*. GEOTRACES Standards and Intercalibration Committee.

Death, R., Wadham, J. L., Monteiro, F., Le Brocq, A. M., Tranter, M., Ridgwell, A., et al. (2014). Antarctic ice sheet fertilises the Southern Ocean. *Biogeosciences*, *11*(10), 2635–2643.

DeJong, H. B., Dunbar, R. B., Koweek, D. A., Mucciarone, D. A., Bercovici, S. K., & Hansell, D. A. (2017). Net community production and carbon export during the late summer in the Ross Sea, Antarctica. *Global Biogeochemical Cycles*, *31*(3), 473–491. https://doi.org/10.1002/2016GB005417

Dinniman, M. S., St-Laurent, P., Arrigo, K. R., Hofmann, E. E., & van Dijken, G. L. (2020). Analysis of iron sources in Antarctic continental shelf waters. *Journal of Geophysical Research: Oceans*, *125*(5), e2019JC015736. https://doi.org/10.1029/2019JC015736

Fitzwater, S. E., Johnson, K. S., Gordon, R. M., Coale, K. H., & Smith, W. O., Jr. (2000). Trace metal concentrations in the Ross Sea and their relationship with nutrients and phytoplankton growth. *Deep Sea Research Part II: Topical Studies in Oceanography*, *47*(15–16), 3159–3179.

Forsch, K. O., Hahn-Woernle, L., Sherrell, R. M., Roccanova, V. J., Bu, K., Burdige, D., et al. (2021). Seasonal dispersal of fjord meltwaters as an important source of iron and manganese to coastal Antarctic phytoplankton. *Biogeosciences*, *18*(23), 6349–6375.

Fusco, G., Budillon, G., & Spezie, G. (2009). Surface heat fluxes and thermohaline variability in the Ross Sea and in Terra Nova Bay polynya. *Continental Shelf Research*, *29*(15), 1887–1895.

Gehlen, M., Beck, L., Calas, G., Flank, A. M., Van Bennekom, A. J., & Van Beusekom, J. E. E. (2002). Unraveling the atomic structure of biogenic silica: Evidence of the structural association of Al and Si in diatom frustules. *Geochimica et Cosmochimica Acta*, *66*(9), 1601–1609.

Gerringa, L. J., Alderkamp, A. C., Van Dijken, G., Laan, P., Middag, R., & Arrigo, K. R. (2020). Dissolved trace metals in the Ross Sea. *Frontiers in Marine Science*, *7*, 874.

Gerringa, L. J. A., Laan, P., Van Dijken, G. L., van Haren, H., De Baar, H. J. W., Arrigo, K. R., & Alderkamp, A. C. (2015). Sources of iron in the Ross Sea polynya in early summer. *Marine Chemistry*, *177*, 447–459.

Giordano, P., Giglio, F., Ravaioli, M., Capello, M., Cutroneo, L., Dunbar, R. B., et al. (2020). *Long time-series of export fluxes in the western Ross Sea (Antarctica)*. Paper presented at the EGU 2020 General Assembly Conference Abstracts 22442.

Gordon, A. L., Zambianchi, E., Orsi, A., Visbeck, M., Giulivi, C. F., Whitworth, T., III., & Spezie, G. (2004). Energetic plumes over the western Ross Sea continental slope. *Geophysical Research Letters*, *31*(21), L21302. https://doi.org/10.1029/2004GL020785

Grotti, M., Soggia, F., Abelmoschi, M. L., Rivaro, P., Magi, E., & Frache, R. (2001). Temporal distribution of trace metals in Antarctic coastal waters. *Marine Chemistry*, *76*(3), 189–209.

Hatta, M., Measures, C. I., Lam, P. J., Ohnemus, D. C., Auro, M. E., Grand, M. M., & Selph, K. E. (2017). The relative roles of modified circumpolar deep water and benthic sources in supplying iron to the recurrent phytoplankton blooms above Pennell and Mawson Banks, Ross Sea, Antarctica. *Journal of Marine Systems*, *166*, 61–72.

Heggie, D., Klinkhammer, G., & Cullen, D. (1987). Manganese and copper fluxes from continental margin sediments. *Geochimica et Cosmochimica Acta*, *51*(5), 1059–1070.

Jackett, D. R., & McDougall, T. J. (1997). A neutral density variable for the world's oceans. *Journal of Physical Oceanography*, *27*(2), 237–263.

Jacobs, S. S., & Giulivi, C. F. (1985). Interannual ocean and sea ice variability in the Ross Sea. *Ocean, Ice, and Atmosphere: Interactions at the Antarctic Continental Margin*, *75*, 135–150.
Jacobs, S. S., Giulivi, C. F., & Dutrieux, P. (2022). Persistent Ross Sea freshening from imbalance West Antarctic ice shelf melting. *Journal of Geophysical Research: Oceans*, *127*(3), e2021JC017808. https://doi.org/10.1029/2021JC017808
Jensen, L. T., Morton, P., Twining, B. S., Heller, M. I., Hatta, M., Measures, C. I., et al. (2020). A comparison of marine Fe and Mn cycling: US GEOTRACES GN01 Western Arctic case study. *Geochimica et Cosmochimica Acta*, *288*, 138–160.
Krisch, S., Hopwood, M. J., Schaffer, J., Al-Hashem, A., Höfer, J., Rutgers van der Loeff, M. M., et al. (2021). The 79°N Glacier cavity modulates subglacial iron export to the NE Greenland Shelf. *Nature Communications*, *12*(1), 1–13.
Kunde, K., Wyatt, N. J., González-Santana, D., Tagliabue, A., Mahaffey, C., & Lohan, M. C. (2019). Iron distribution in the subtropical North Atlantic: The pivotal role of colloidal iron. *Global Biogeochemical Cycles*, *33*(12), 1532–1547. https://doi.org/10.1029/2019GB006326
Kwok, R. (2005). Ross Sea ice motion, area flux, and deformation. *Journal of Climate*, *18*(18), 3759–3776.
Kwon, E. Y., Primeau, F., & Sarmiento, J. L. (2009). The impact of remineralization depth on the air–sea carbon balance. *Nature Geoscience*, *2*(9), 630–635.
Lagerström, M. E., Field, M. P., Séguret, M., Fischer, L., Hann, S., & Sherrell, R. M. (2013). Automated on-line flow-injection ICP-MS determination of trace metals (Mn, Fe, Co, Ni, Cu and Zn) in open ocean seawater: Application to the GEOTRACES program. *Marine Chemistry*, *155*, 71–80.
Lancelot, C., de Montety, A., Goosse, H., Becquevort, S., Schoemann, V., Pasquer, B., & Vancoppenolle, M. (2009). Spatial distribution of the iron supply to phytoplankton in the Southern Ocean: A model study. *Biogeosciences*, *6*(12), 2861–2878.
Lannuzel, D., Vancoppenolle, M., Van der Merwe, P., De Jong, J., Meiners, K. M., Grotti, M., et al. (2016). Iron in sea ice: Review and new insights. *Elementa: Science of the Anthropocene*, *4*, 000130.
Laufkoetter, C., Stern, A. A., John, J. G., Stock, C. A., & Dunne, J. P. (2018). Glacial iron sources stimulate the Southern Ocean carbon cycle. *Geophysical Research Letters*, *45*(24), 13377–13385. https://doi.org/10.1029/2018GL079797
Loose, B., Stammerjohn, S., Sedwick, P., Delille, B., & Ackley, S. (2022). Sea ice formation, glacial melt and the solubility pump boundary conditions in the Ross Sea. *Journal of Geophysical Research: Oceans*. In press. https://doi.org/10.1002/essoar.10512535.1
Mack, S. L., Dinniman, M. S., McGillicuddy, D. J., Jr., Sedwick, P. N., & Klinck, J. M. (2017). Dissolved iron transport pathways in the Ross Sea: Influence of tides and horizontal resolution in a regional ocean model. *Journal of Marine Systems*, *166*, 73–86.
Manzella, G. M. R., Meloni, R., & Picco, P. (1999). Current, temperature and salinity observations in the Terra Nova Bay polynya area. In *Oceanography of the Ross Sea Antarctica* (pp. 165–173). Springer.
Marinov, I., Gnanadesikan, A., Toggweiler, J. R., & Sarmiento, J. L. (2006). The Southern Ocean biogeochemical divide. *Nature*, *441*(7096), 964.
Marsay, C. M., Barrett, P. M., McGillicuddy, D. J., Jr., & Sedwick, P. N. (2017). Distributions, sources, and transformations of dissolved and particulate iron on the Ross Sea continental shelf during summer. *Journal of Geophysical Research: Oceans*, *122*(8), 6371–6393. https://doi.org/10.1002/2017JC013068
Marsay, C. M., Sedwick, P. N., Dinniman, M. S., Barrett, P. M., Mack, S. L., & McGillicuddy, D. J., Jr. (2014). Estimating the benthic efflux of dissolved iron on the Ross Sea continental shelf. *Geophysical Research Letters*, *41*(21), 7576–7583. https://doi.org/10.1002/2014GL061684
Martin, J. H., Gordon, R. M., & Fitzwater, S. E. (1990). Iron in Antarctic waters. *Nature*, *345*(6271), 156–158.
McGillicuddy, D. J., Jr., Sedwick, P. N., Dinniman, M. S., Arrigo, K. R., Bibby, T. S., Greenan, B. J. W., et al. (2015). Iron supply and demand in an Antarctic shelf ecosystem. *Geophysical Research Letters*, *42*(19), 8088–8097. https://doi.org/10.1002/2015GL065727
Measures, C. I., Brown, M. T., Selph, K. E., Apprill, A., Zhou, M., Hatta, M., & Hiscock, W. T. (2013). The influence of shelf processes in delivering dissolved iron to the HNLC waters of the Drake Passage, Antarctica. *Deep Sea Research Part II: Topical Studies in Oceanography*, *90*, 77–88.
Meehl, G. A., Arblaster, J. M., Chung, C. T., Holland, M. M., DuVivier, A., Thompson, L., et al. (2019). Sustained ocean changes contributed to sudden Antarctic Sea ice retreat in late 2016. *Nature Communications*, *10*(1), 1–9.
Middag, R., De Baar, H. J. W., Laan, P., & Huhn, O. (2012). The effects of continental margins and water mass circulation on the distribution of dissolved aluminum and manganese in Drake Passage. *Journal of Geophysical Research*, *117*(C1), C01019.
Milne, A., Landing, W., Bizimis, M., & Morton, P. (2010). Determination of Mn, Fe, Co, Ni, Cu, Zn, Cd and Pb in seawater using high resolution magnetic sector inductively coupled mass spectrometry (HR-ICP-MS). *Analytica Chimica Acta*, *665*(2), 200–207.
Oldham, V. E., Chmiel, R., Hansel, C. M., DiTullio, G. R., Rao, D., & Saito, M. (2021). Inhibited manganese oxide formation hinders cobalt scavenging in the Ross Sea. *Global Biogeochemical Cycles*, *35*(5), e2020GB006706. https://doi.org/10.1029/2020GB006706
Orsi, A. H., & Wiederwohl, C. L. (2009). A recount of Ross Sea waters. *Deep Sea Research Part II: Topical Studies in Oceanography*, *56*(13–14), 778–795.
Parkinson, C. L. (2019). A 40-y record reveals gradual Antarctic Sea ice increases followed by decreases at rates far exceeding the rates seen in the Arctic. *Proceedings of the National Academy of Sciences of the United States of America*, *116*(29), 14414–14423.
Person, R., Aumont, O., Madec, G., Vancoppenolle, M., Bopp, L., & Merino, N. (2019). Sensitivity of ocean biogeochemistry to the iron supply from the Antarctic Ice Sheet explored with a biogeochemical model. *Biogeosciences*, *16*(18), 3583–3603.
Person, R., Vancoppenolle, M., & Aumont, O. (2020). Iron incorporation from seawater into Antarctic Sea ice: A model study. *Global Biogeochemical Cycles*, *34*(11), e2020GB006665. https://doi.org/10.1029/2020GB006665
Person, R., Vancoppenolle, M., Aumont, O., & Malsang, M. (2021). Continental and sea ice iron sources fertilize the Southern Ocean in synergy. *Geophysical Research Letters*, *48*, e2021GL094761. https://doi.org/10.1029/2021GL094761
Piñones, A., Hofmann, E. E., Costa, D. P., Goetz, K., Burns, J. M., Roquet, F., et al. (2019). Hydrographic variability along the inner and mid-shelf region of the Western Ross Sea obtained using instrumented seals. *Progress in Oceanography*, *174*, 131–142.
Porter, D. F., Springer, S. R., Padman, L., Fricker, H. A., Tinto, K. J., Riser, S. C., et al. (2019). Evolution of the seasonal surface mixed layer of the Ross Sea, Antarctica, observed with autonomous profiling floats. *Journal of Geophysical Research: Oceans*, *124*(7), 4934–4953. https://doi.org/10.1029/2018JC014683
Rack, W., Price, D., Haas, C., Langhorne, P. J., & Leonard, G. H. (2021). Sea ice thickness in the Western Ross Sea. *Geophysical Research Letters*, *48*(1), e2020GL090866. https://doi.org/10.1029/2020GL090866
Rusciano, E., Budillon, G., Fusco, G., & Spezie, G. (2013). Evidence of atmosphere–sea ice–ocean coupling in the Terra Nova Bay polynya (Ross Sea—Antarctica). *Continental Shelf Research*, *61*, 112–124.
Schlosser, E., Haumann, F. A., & Raphael, M. N. (2018). Atmospheric influences on the anomalous 2016 Antarctic Sea ice decay. *The Cryosphere*, *12*(3), 1103–1119.
Sedwick, P. N., DiTullio, G. R., & Mackey, D. J. (2000). Iron and manganese in the Ross Sea, Antarctica: Seasonal iron limitation in Antarctic shelf waters. *Journal of Geophysical Research*, *105*(C5), 11321–11336.

Sedwick, P. N., Marsay, C. M., Sohst, B. M., Aguilar-Islas, A. M., Lohan, M. C., Long, M. C., et al. (2011). Early season depletion of dissolved iron in the Ross Sea polynya: Implications for iron dynamics on the Antarctic continental shelf. *Journal of Geophysical Research*, *116*(C12), C12019.

Sherrell, R. M., Annett, A. L., Fitzsimmons, J. N., Roccanova, V. J., & Meredith, M. P. (2018). A 'shallow bathtub ring' of local sedimentary iron input maintains the Palmer Deep biological hotspot on the West Antarctic Peninsula shelf. *Philosophical Transactions of the Royal Society A: Mathematical, Physical & Engineering Sciences*, *376*(2122), 20170171.

Smethie, W. M., Jr., & Jacobs, S. S. (2005). Circulation and melting under the Ross Ice Shelf: Estimates from evolving CFC, salinity and temperature fields in the Ross Sea. *Deep Sea Research Part I: Oceanographic Research Papers*, *52*(6), 959–978.

Smith, W. O., Jr., Sedwick, P. N., Arrigo, K. R., Ainley, D. G., & Orsi, A. H. (2012). The Ross Sea in a sea of change. *Oceanography*, *25*(3), 90–103.

St-Laurent, P., Yager, P. L., Sherrell, R. M., Oliver, H., Dinniman, M. S., & Stammerjohn, S. E. (2019). Modeling the seasonal cycle of iron and carbon fluxes in the Amundsen Sea Polynya, Antarctica. *Journal of Geophysical Research: Oceans*, *124*(3), 1544–1565. https://doi.org/10.1029/2018JC014773

St-Laurent, P., Yager, P. L., Sherrell, R. M., Stammerjohn, S. E., & Dinniman, M. S. (2017). Pathways and supply of dissolved iron in the Amundsen Sea (Antarctica). *Journal of Geophysical Research: Oceans*, *122*(9), 7135–7162. https://doi.org/10.1002/2017JC013162

Tagliabue, A., & Arrigo, K. R. (2005). Iron in the Ross Sea: 1. Impact on CO2 fluxes via variation in phytoplankton functional group and non-Redfield stoichiometry. *Journal of Geophysical Research*, *110*(C3), C03009.

Tagliabue, A., & Arrigo, K. R. (2006). Processes governing the supply of iron to phytoplankton in stratified seas. *Journal of Geophysical Research*, *111*(C6), C06019.

Thompson, L., Smith, M., Thomson, J., Stammerjohn, S., Ackley, S., & Loose, B. (2020). Frazil ice growth and production during katabatic wind events in the Ross Sea, Antarctica. *The Cryosphere*, *14*(10), 3329–3347.

Thuróczy, C. E., Alderkamp, A. C., Laan, P., Gerringa, L. J., Mills, M. M., Van Dijken, G. L., et al. (2012). Key role of organic complexation of iron in sustaining phytoplankton blooms in the Pine Island and Amundsen Polynyas (Southern Ocean). *Deep Sea Research Part II: Topical Studies in Oceanography*, *71*, 49–60.

Turner, J., Phillips, T., Marshall, G. J., Hosking, J. S., Pope, J. O., Bracegirdle, T. J., & Deb, P. (2017). Unprecedented springtime retreat of Antarctic Sea ice in 2016. *Geophysical Research Letters*, *44*(13), 6868–6875. https://doi.org/10.1002/2017GL073656

Vance, D., Little, S. H., de Souza, G. F., Khatiwala, S., Lohan, M. C., & Middag, R. (2017). Silicon and zinc biogeochemical cycles coupled through the Southern Ocean. *Nature Geoscience*, *10*(3), 202–206.

Wang, S., Bailey, D., Lindsay, K., Moore, J. K., & Holland, M. (2014). Impact of sea ice on the marine iron cycle and phytoplankton productivity. *Biogeosciences*, *11*(17), 4713–4731.

Yoon, S. T., Lee, W. S., Stevens, C., Jendersie, S., Nam, S., Yun, S., et al. (2020). Variability in high-salinity shelf water production in the Terra Nova Bay polynya, Antarctica. *Ocean Science*, *16*(2), 373–388.